3068–3085 *Nucleic Acids Research, 2017, Vol. 45, No. 6* *Published online 9 December 2016*
doi: 10.1093/nar/gkw1244

The Drosophila telomere-capping protein Verrocchio binds single-stranded DNA and protects telomeres from DNA damage response

Alessandro Cicconi[1,2,†], Emanuela Micheli[1,2,†], Fiammetta Vernì[1], Alison Jackson[3], Ana Citlali Gradilla[3], Francesca Cipressa[1,2,4], Domenico Raimondo[5], Giuseppe Bosso[1,2], James G. Wakefield[3], Laura Ciapponi[1], Giovanni Cenci[1,2], Maurizio Gatti[1,6], Stefano Cacchione[1,2,*] and Grazia Daniela Raffa[1,2,*]

[1]Dipartimento di Biologia e Biotecnologie 'C. Darwin', Sapienza, Università di Roma, 00185 Roma, Italy, [2]Istituto Pasteur Italia - Fondazione Cenci Bolognetti, 00185 Roma, Italy, [3]Biosciences, College of Life and Environmental Sciences, University of Exeter, Exeter EX4 4QD, UK, [4]Centro Fermi, Piazza del Viminale 1, 00184 Roma, Italy, [5]Dipartimento di Medicina Molecolare, Sapienza, Università di Roma, 00185 Roma, Italy and [6]Istituto di Biologia e Patologia Molecolari (IBPM) del CNR, 00185 Roma, Italy

Received April 13, 2016; Revised November 22, 2016; Editorial Decision November 24, 2016; Accepted November 28, 2016

ABSTRACT

Drosophila **telomeres are sequence-independent structures maintained by transposition to chromosome ends of three specialized retroelements rather than by telomerase activity. Fly telomeres are protected by the terminin complex that includes the HOAP, HipHop, Moi and Ver proteins. These are fast evolving, non-conserved proteins that localize and function exclusively at telomeres, protecting them from fusion events. We have previously suggested that terminin is the functional analogue of shelterin, the multi-protein complex that protects human telomeres. Here, we use electrophoretic mobility shift assay (EMSA) and atomic force microscopy (AFM) to show that Ver preferentially binds single-stranded DNA (ssDNA) with no sequence specificity. We also show that Moi and Ver form a complex in vivo. Although these two proteins are mutually dependent for their localization at telomeres, Moi neither binds ssDNA nor facilitates Ver binding to ssDNA. Consistent with these results, we found that Ver-depleted telomeres form RPA and γH2AX foci, like the human telomeres lacking the ssDNA-binding POT1 protein. Collectively, our findings suggest that *Drosophila* telomeres possess a ssDNA overhang like the other eukaryotes, and that the terminin complex is architecturally and functionally similar to shelterin.**

INTRODUCTION

Dealing with chromosome ends represents a major problem for the cell, as they can be mistaken for double strand breaks (DSBs) and activate the DNA damage response (DDR), leading to unwanted repair, telomere fusion and genome instability. Different organisms evolved different protein complexes that specifically bind chromosome ends and help assembly of the telomere, a protective structure that shields DNA termini preventing DSB signaling. In most eukaryotes, telomeric DNA consists of short tandem repeats added by telomerase to chromosome ends (1,2). Replication of the lagging strand results in the formation of a terminal 3′ G-rich overhang (3); completion of telomere replication through a fine interplay between exonuclease activities and fill-in DNA synthesis results in 3′ overhangs of appropriate length at the ends of both sister chromatids (4,5).

In organisms with telomerase, terminal repeats are specifically recognized by specialized telomere capping complexes (6). In humans, the TTAGGG repeats are selectively bound by the six-protein (TRF1, TRF2, Rap1, TIN2, TPP1, POT1) shelterin complex, which localizes and function almost exclusively at telomeres (7,8). TRF1 and TRF2 bind the TTAGGG duplex and POT1 the 3′ overhang; TIN2 and TPP1 bridge POT1 to TRF1 and TRF2. hRap1, a distant homologue of *Saccharomyces cerevisiae* Rap1, interacts with TRF2, but is not directly implicated in telomere protection or length regulation (9). TRF2 dysfunction triggers the ATM signaling pathway, and leads to the accumulation of telomere dysfunction foci (TIFs) enriched in γ-H2AX (10–12). Loss of POT1 causes the accumulation

*To whom correspondence should be addressed. Tel: +39 06 49912238; Fax +39 06 49912351; Email: stefano.cacchione@uniroma1.it
Correspondence may also be addressed to Grazia Daniela Raffa. Tel: +39 06 49912843; Fax: +39 06 49912343; Email: graziadaniela.raffa@uniroma1.it
†These authors contributed equally to this work as first authors.

of RPA (Replication protein A) onto the 3′ overhang, which activates the ATR signaling pathway and leads to TIFs (13–17). RPA is normally recruited at telomere overhangs during DNA replication, at a time when POT1 is partially released from the telomere, but is replaced by POT1 at the end of DNA replication. Interestingly, transient ATM- and ATR-mediated DNA damage signaling occurs even at normal human telomeres that are completing DNA replication (18).

Although 3′ overhangs are prevalent among telomeres of organisms with telomerase, in *Caenorhabditis elegans* 5′ overhangs are as abundant as 3′ overhangs (19), and blunt-ended telomeres have been found in *Arabidopsis thaliana* (20). 5′ overhangs have been also found in mouse and human cells, particularly in G1/S arrested and terminally differentiated cells, as well as in cancer cells that exploit the alternative lengthening of telomeres (ALT) pathway for telomere maintenance (21).

In fission yeast, telomeric DNA is protected by a complex that is architecturally reminiscent of shelterin and contains the TRF1 and POT1 homologues Taz1 and SpPot1 (22–24). In budding yeast, there is not a shelterin complex and the shelterin functions are fulfilled by Rap1 and the RPA-like complex Cdc13-Stn1-Ten1 (CST) (25,26). Cdc13 does not share homology with POT1, but both proteins use oligonucleotide/oligosaccharide-binding (OB)-fold domains to bind ssDNA. The CST complex exists also in mammals, where it coordinates telomerase-mediated DNA elongation and fill-in synthesis during telomere replication (27–29); however, its function is not restricted to telomeres, as it also plays a general role in DNA replication (30,31).

In *Drosophila,* there is not telomerase and telomeres are elongated by the targeted transposition of three specialized non-LTR retrotransposons (HeT-A, TART and TAHRE) (32–35). In addition, abundant evidence indicates that *Drosophila* telomeres can assemble independently of the sequence of the DNA termini (36–38). *Drosophila* telomeres are capped and protected by the terminin complex, which includes HOAP, Moi and Ver. All these proteins interact with each other and share the same features as the shelterin subunits: they are specifically enriched at telomeres throughout the cell cycle and do not perform other functions elsewhere in the genome (32,39–41). Most likely, terminin also includes HipHop, another fast evolving protein that interacts with HOAP and shares the shelterin-like properties of HOAP, Moi and Ver (32,42).

Here we focus on the Verrocchio (Ver) protein, which contains an OB-fold domain with structural similarity to Stn1/RPA2 OB fold (40). Ver interacts with Modigliani (Moi), and Moi and Ver are both HOAP-dependent and mutually dependent for their telomeric localization (39,40). Ver has been also implicated in the recruitment of the HeT-A encoded ORF1p protein and HeT-A transcripts at the telomere (43). Here, we use both electrophoretic mobility shift assay (EMSA) and atomic force microscopy (AFM) to show that Ver binds ssDNA *in vitro*. We also show that Moi does not bind DNA and that Ver interaction with Moi is necessary for Ver localization at telomeres but not for its binding to ssDNA. Finally, we demonstrate that loss of Ver favors RPA accumulation at telomeres and triggers DNA damage signaling. This suggests that Ver is a functional analog of ssDNA binding proteins such as yeast Cdc13 and human POT1.

MATERIALS AND METHODS

Drosophila strains

The *ver*^{1} and *moi*^{1} alleles and the Ver-GFP expressing flies have been described previously (39,40). The Oregon-R or the ywf strains were used as wild type controls. All flies were reared according to standard procedures and maintained at 25°C. The Histone-H3-RFP strain was obtained by the Bloomington stock center.

Generation of Ver$^{\Delta C}$-GFP and GFP-RPA expressing flies

To generate Ver$^{\Delta C}$-GFP expressing flies, the EGFP CDS was fused in frame with the 3′-end of the Ver$^{\Delta C}$ (aa 1–185) CDS. The resulting construct was cloned into the pJZ4 vector (a derivative of pCASPER4), under the control of a tubulin promoter (39,40). To generate flies carrying an inducible *UAS-GFP-RpA70* transgene, the *RPA70* CDS was first cloned in the pENTR vector (pENTR™/D-TOPO® Cloning Kit, ThermoFisher Scientific) and then cloned in frame to the EGFP CDS in the ppGW vector (Drosophila Gateway™ Vector Collection, Carnegie Institution for Science), using the Gateway® LR Clonase® II Enzyme mix, (ThermoFisher Scientific). Germline transformation was carried out by the BestGene Company (Indiana, USA) using standard methods. Flies ubiquitously expressing GFP-RPA70 were obtained through appropriate crosses between the *UAS-GFP-RpA70* flies and flies expressing the actin-GAL4 driver (B#25374, obtained from the Bloomington stock Center).

Protein purification

To obtain the GST-Ver$^{\Delta C}$ fusion protein, the *ver* region coding for aa 1–185 was cloned in pGEX-6P vector as described previously for GST-Ver and GST-Moi (39,40). GST fusion proteins were expressed in the BL21 strain (DE3), purified by incubating crude lysates with glutathione-sepharose 4B (Amersham), and eluted with 50 mM Tris–HCl, 10 mM reduced glutathione, pH 8.0. Recombinant His–Ver protein was also expressed in the BL21 strain (DE3) (40). Exponentially growing bacteria were induced at 37°C for 4 h by addition of 2 mM IPTG. Bacteria were harvested, resuspended and incubated for 1 h in lysis buffer (400 mM NaCl, 100 mM KCl, 10% glycerol, 0.5% Triton X-100, 10 mM Imidazole, 50 mM Phosphate buffer pH 7.8, 0.2% lysozime, Complete protease inhibitors Roche). Lysates were then sonicated for 20 s, incubated for 30 min with 1.5% *N*-lauryl sarcosyn, and centrifuged for 25 min at 4°C. The soluble portion was then incubated for 1 h with the Ni-NTA His-Bind Resin (Qiagen), extensively washed with lysis buffer containing 20 mM imidazole, and eluted with lysis buffer containing 250 mM imidazole. Protein concentrations were calculated using the Bradford assay (Sigma). The purity of the isolated proteins has been verified by SDS-PAGE electrophoresis followed by Coomassie staining (Supplementary Figure S1).

Preparation of DNA constructs

Oligonucleotides, obtained from Bio-Fab Research, are listed in Supplementary Table S1. For EMSA, oligonucleotides were radiolabeled with [γ-^{32}P] using T4 polynucleotide kinase and purified using the QIAquick Nucleotide Removal Kit (Qiagen). To generate 3′-tail DNA, 5′-tail DNA and duplex DNA constructs, ss60-1 was annealed with ss30-3, ss30-4 and ss60-2, respectively (see Supplementary Table S1); annealing was performed in 100 mM NaCl, 10 mM Tris–HCl, 1 mM EDTA pH 8.0, by denaturing the samples at 95°C for 10 min and then gradually decreasing the temperature.

For AFM imaging, the Blunt-end construct (BEC) was obtained by digesting pUC18 DNA with DraI (Thermoscientific). The digested sample was run on a 1% agarose gel and the 694 bp blunt DNA fragment was purified with QIAquick gel-extraction kit (Qiagen). To obtain the 3′-single-tail DNA construct (3′-STC), a DNA fragment of 1246 bp was amplified by PCR from the pUC18 plasmid (primers 1246-fw and 1246-rv), and digested with PstI (Thermo Scientific), obtaining two fragments (400 and 842 bp) with a blunt end and a 4-nt 3′-OH protruding end. The 842 bp fragment was gel-purified and then ligated to the adapter resulting from the annealing of the 60-nt long oligonucleotide ss60-1 and the 22 nt long Ada-3′. The ligated 3′-STC contained a blunt end and a 42-nt 3′-protruding end. To obtain the 3′-Double-tail DNA construct (3′-DTC), a 1216 bp DNA fragment, derived from pUC18 digestion with Alw44I, was ligated to an adapter formed by the 68-nt long oligonucleotide DT68 and Ada-3′. The resulting 3′-DTC fragment consisted of 1260 bp with 42-nt overhang at both ends. The 5′-double-tail DNA construct (5′-DTC) was obtained by ligating a 943 bp DNA fragment, derived from pUC18 digestion with Alw44I, with an adapter formed by ss60-1 oligonucleotide and the 22-nt long Ada-5′. The resulting 5′-DTC fragment was 979-bp long, with 42-nt overhang at both ends.

Electrophoretic mobility shift assay

Protein-DNA binding reactions were carried out in 20 μl of binding buffer (50 mM HEPES–KOH pH 7.8, 50 mM KCl, 0.1 mM EDTA, 5% glycerol, 0.2% NP40, 1 mM DTT, 0.1 μg/μl BSA) for 60 min at 4°C, and run on native 5% acrylamide/bis acrylamide gels [19:1] at 4°C for 2 h in 0.5× TBE at 150V. Gels were dried and analyzed with a phosphorimager apparatus (Typhoon, GE Healthcare). Crosslinking reaction were carried out by adding 0.1% glutaraldehyde during the last 10 min of the binding reaction. Binding competitions were carried out by adding to the reaction 1 μM unlabeled DNA (see Figure legends for details).

WEMSA assay

EMSA was performed as described above using labeled and unlabeled ss30-1 and GST-Ver. After electrophoresis, the 8% polyacrylamide gel was cut into two halves; the part with the labeled probe was dried and analysed with a phosphoimager apparatus, while the part with the unlabeled probe was transferred to a nitrocellulose membrane (Hybond ECL, Amersham) by electroblotting. The membrane was then hybridized with anti-GST HRP-conjugated antibody (1:5000, GE Healthcare) to visualize GST-Ver.

AFM imaging

AFM imaging of DNA-protein complexes was performed as previously described (44,45). 10 nM of each DNA construct was incubated for 30 min at 4°C with 200 nM 6His–Ver or 10 nM SSB in AFM binding buffer (50 mM HEPES–KOH pH 7.8, 50 mM KCl, 0.1 mM EDTA, 1 mM DTT) in a total volume of 20 μl. Samples were then crosslinked by addition of 0.1% glutaraldehyde for 30 minutes on ice, and the DNA–protein complexes were purified using the QIAquick PCR Purification Kit (Qiagen). 10 μl of purified samples in AFM imaging buffer (4 mM HEPES–KOH pH 7.5, 10 mM NaCl, 1.5 mM $MgCl_2$) were deposited at the center of freshly cleaved mica. Spreading of samples on the substrate was performed in the presence of Mg^{2+}, to promote adhesion of DNA/protein complexes to negatively charged mica (46). After 1 min, the mica surface was rinsed with deionized water and dried under a gentle nitrogen flow. The concentrations of the DNA-protein complexes were adjusted in order to have a uniform spreading of the molecules with no overlaps (the images reported here have been taken at 0.5 nM concentration of the DNA/protein complex). DNA constructs and proteins alone were also deposited on mica, in AFM imaging buffer at 0.5 and 1.4 nM concentration, respectively. AFM imaging was performed on a MultiMode SPM Nanoscope Digital III A, equipped with E-scanner (Digital Instruments Inc., Santa Barbara, CA, USA), operating in tapping mode at room temperature, using canonical sharp silicon tips (Veeco). Images of 512 × 512 pixels were recorded at a scanning rate of 1.5–2.0 Hz in a scan area 1–3 μm wide.

Analysis of AFM data

To evaluate DNA contour lengths, AFM images were converted from Nanoscope format into TIF files and processed using the ImageJ software. To assess Ver position along the constructs, we determined the distance between the center of the bound protein and the closest DNA end (L_1) (see Figure 2B); for proteins bound at the ends of the constructs, L_1 was considered 0. Half-length constructs were then divided into 10.2 nm-long sections (∼30 bp), and the proteins assigned to each section using L_1. To determine whether the observed protein binding distributions were different from continuous uniform distributions we used the χ^2 test. To assess whether Ver binds the ssDNA overhangs (which are not visible in AFM images) the contour length of end-bound DNA molecules (L_2) was measured starting from the outer edge of the protein, and was then compared with the contour lengths of free DNA molecules (L) (see Figure 4). The histograms obtained from contour length measurements were fitted to Gaussian function using the open source QtiPlot software. To determine whether L is statistically different from L_2 we used the Student's t-test. Protein volume was measured using the open source WSXM software. Volumes were calculated considering the proteins as hemi-ellipsoids using the formula: $V = \frac{4}{6}\pi r_1 r_2 h$; where r_1 and r_2 represent respectively the major and the minor radii of the protein

section at half height, and h represents the mean protein height from the background (47,48). Since it is known that SSB binds ssDNA as a tetramer (4 × 18.8 kDa) (49), the volume found for bound SSB (100 nm^3) was used as a standard to elaborate a conversion coefficient (1.33 nm^3/kDa) to derive the expected Ver volumes from the mass of 6His–Ver protein (28.5 kDa).

Chromosome cytology and immunostaining

Preparation and immunostaining of mitotic chromosomes have been described previously (50,51). To obtain polytene chromosomes for immunostaining, salivary glands from third instar larvae were dissected and incubated for 8 min in G Medium (25 mM sodium glycerophosphate, 10 mM KH_2PO_4, 30 mM KCl, 10 mM $MgCl_2$, 3 mM $CaCl_2$, 160 mM sucrose, 0.5% NP40), fixed for 20 min in (100 mM NaCl, 2 mM KCl, 10 mM sodium phosphate buffer pH 7, 2.8% formaldehyde, 2% NP-40), transferred for 10 min to 45% acetic acid and squashed in the same solution. Slides were frozen in liquid nitrogen and, after flipping off the coverslip, immediately immersed in cold TBS for 5 min. Slides were then washed in TBS-T (TBS containing 0.05% Tween 20) and incubated overnight at 4°C with mouse anti-γH2AV (1:20, DSHB, Iowa) and either rabbit anti-HOAP (generated in our laboratory; 1:20), or rabbit anti-GFP (1:100, Torrey Pines Biolabs). Secondary antibody incubation was carried out at room temperature for 1 h using FITC-conjugated anti-rabbit (1:50, Jackson Immunoresearch) and AlexaFluor 555-conjugated anti-mouse (1:50, ThermoFisher Scientific). Slides were mounted in Vectashield H-1200 with DAPI to stain DNA. Polytene chromosome preparations were analyzed using a Zeiss Axioplan epifluorescence microscope equipped with a cooled CCD camera (CoolSnap, Photometrics). To quantify the relative intensities of the γH2AV and HOAP signals at the polytene chromosome telomeres, we measured separately each signal and subtracted the relative background using the ImageJ software. We then calculated the ratio between the γH2AV and HOAP fluorescence. Notably, this calculation precisely corresponded to a visual evaluation of the two signals; any time the γH2AV/HOAP fluorescence ratio was >1, the γH2AV signal was more extended than the HOAP signal.

GFP-TRAP-A based AP-MS of Ver-GFP

Batches of 0–3 h old embryos laid by cages of 1–10 day-old Ver-GFP flies were dechorionated, weighed, flash frozen in liquid nitrogen and stored at -80 °C. For MS analysis, ∼0.4 g of frozen embryos were homogenized in 1.5 ml of C buffer (50 mM HEPES [pH 7.4], 50 mM KCl, 1 mM $MgCl_2$, 1 mM EGTA, 0.1% IGEPAL CA-630, protease inhibitors (Roche). Extract was clarified through centrifugation at 10 000 g for 10 min, 100 000 g for 30 min and 100 000 g for a further 10 min. Clarified extract was incubated with 30 μl GFP-TRAP-A beads equilibrated in C Buffer (Chromotek) for 2 h at 4°C. Beads were then washed 4 times with ice-cold C buffer and stored at -20°C. Mass spectrometric analysis was undertaken by the Bristol Proteomics Facility (http://www.bristol.ac.uk/biomedical-sciences/research/facilities/proteomics/), essentially following the procedure described in (52). The resultant raw data files were processed and quantified using Proteome Discoverer software v1.2 (Thermo Scientific) and searched against the dmel-all-translation-r5.47 database using the SEQUEST (Ver. 28 Rev. 13) algorithm. Peptide precursor mass tolerance was set at 10ppm, and MS/MS tolerance was set at 0.8Da. Search criteria included carbamidomethylation of cysteine (+57.0214) as a fixed modification and oxidation of methionine (+15.9949) as a variable modification. Searches were performed with full tryptic digestion and a maximum of one missed cleavage was allowed. The reverse database search option was enabled and all peptide data were filtered to satisfy false discovery rate (FDR) of 5%. To remove non-specific interacting proteins, the list of protein IDs was cross-referenced with our false-positive list (52). IDs not present in the false-positive list, or those enriched in the experimental sample by >3 fold, were kept; all other IDs were removed. The proteins were further filtered by removing protein IDs with overall MS Scores <50 and Areas <1:100 (0.01) Bait: Interacting protein. A less stringent filtering of this dataset (showing all specific proteins identified with MS scores of >50) can be found on the Wakefield lab website (www.thewakefieldlab.com/MS).

In vivo imaging

For *in vivo* time-lapse imaging of embryos, dechorionated 1–2 h old embryos expressing Ver-GFP and Histone-H3-RFP were aligned in heptane glue on 22 × 50 mm coverslips, and covered with a 1:1 mixture of Halocarbon oil 700 and Halocarbon oil 27 (Sigma). Imaging was performed using a Visitron Systems Olympus IX81 microscope equipped with a CSO-X1 spinning disk using a UPlanS APO 1.3 NA (Olympus) 60X objective. Five-1μm slice stacks were acquired at a 400 ms exposure per slice, at a constant room temperature of 22°C. Image processing and analysis was performed using ImageJ to produce accumulated projections.

GST pull-down assays

Bacterially expressed GST-Ver and GST-$Ver^{\Delta C}$ fusion proteins were purified by incubating crude lysates with glutathione sepharose 4B (Amersham), as recommended by the manufacturer. 6His–Ver was generated and purified from bacteria as described above. GST pull-down was performed as described previously (40). 6His–Ver was detected with anti-His HRP-conjugated (1:500; Roche) antibody.

Co-immunoprecipitation

The *RPA-FLAG* construct was obtained by cloning the RPA-70 coding sequence, fused in frame to a sequence encoding the 3XFLAG peptide, into the pJZ4 plasmid. S2 cells were transfected with plasmids encoding GFP-Ver and RPA70-FLAG using the Effectene Transfection Reagent (Qiagen). After 3 days, 5 ml of cell suspension were pelleted and incubated for 30 min on ice in 500 μl of lysis buffer (150 mM NaCl, 50 mM Tris–HCl pH 7.5, 30 mM NaF, 25 mM β-glycerophosphate, 10 mM Na_3VO_4, 1% Triton X-100, 0.5 mM PMSF, 1× protease inhibitor cocktail). After

centrifugation for 10 min at 13 000 rpm at 4°C, the pellet was resuspended in 250 μl of lysis buffer and the nuclei were lysed using a syringe, and sonicated for 10 s. The lysate was then clarified by centrifugation. For DNase I-treated samples, the lysate was incubated for 30 min at 37°C with 1U of DNase I (ThermoFisher Scientific). 4% of each lysate was retained as the 'input', while the remainder was incubated with 15 μl of either ANTI-FLAG M2 Affinity Gel (Sigma-Aldrich) or GFP-Trap (Chromotek) beads for 2 h at 4°C. The beads were washed four times with 0.5% Triton X-100 containing PBS, boiled in SDS sample buffer and separated by SDS-PAGE. For immunoblotting, rabbit anti-GFP (1:1500, Torrey Pines Biolabs) and anti-FLAG HRP-conjugated (1:200, Roche) were used to detect GFP-Ver and RPA-FLAG, respectively.

RESULTS

Ver binds ssDNA *in vitro* in a sequence-independent fashion

To test whether Ver has the ability to bind ssDNA in a sequence-independent manner, we performed EMSA experiments by incubating bacterially purified GST-Ver with terminally labeled oligonucleotides (oligos) of random sequence (Supplementary Table S1). We used two different 30-mer oligos (ss30-1 and ss30-2). When increasing amounts of GST-Ver were incubated with either oligo, protein/DNA complexes formed, although a consistent fraction of the DNA probe remained unbound even at the highest protein concentration (Figure 1A and B). We usually observed two complexes (also after glutaraldehyde crosslinking); they might reflect either different conformations of the complexes or different binding modes. We confirmed that the retarded complexes contain the Ver protein using a combined western blot/electrophoretic mobility assay (WEMSA) (53,54). The GST-Ver/ss30-1 complexes run on a polyacrylamide gel were transferred on a nitrocellulose membrane and immunoblotted with an anti-GST antibody. We detected a strong GST signal matching the complex of the EMSA experiment (Supplementary Figure S2, lanes 2 and 4). To determine whether Ver specifically binds ssDNA, we performed EMSA in the presence of competitor DNA: 100-fold excess of unlabeled ssDNA (ss30-2 oligo) or double-stranded DNA (calf thymus DNA). Whereas ssDNA efficiently competed with the ss30-1 oligo in binding GST-Ver (Figure 1A, lane 7), dsDNA did not inhibit the formation of GST-Ver/ss30-1 complex (Figure 1A, lane 8).

We next investigated Ver binding to DNA fragments that mimic the chromosome end structure of organisms with telomerase, namely dsDNAs ending with a protruding ss-overhang. In this analysis we tested DNAs consisting of 30 bp-long duplexes with 30 nt-long 3′- or 5′-protruding ssDNA tails (abbreviated with 3′-tail and 5′-tail, see Supplementary Table S1), as we wanted to determine whether Ver was preferentially binding one of the two types of overhangs. As shown in Figures 1C and Supplementary Figure S3, GST-Ver binds with similar affinity the 3′-tail and 5′-tail probes but fails to bind a double-stranded 60 bp probe used as control.

Collectively, these results indicate that Ver binds ssDNA in a sequence-independent manner, although with low affinity. This low binding affinity prevented an accurate estimate of the dissociation constant.

Atomic force microscopy (AFM) reveals that Ver binds ssDNA as a dimer

To confirm that Ver binds ssDNA, we visualized Ver–DNA complexes by AFM. AFM allows definition of the position of a DNA-binding protein along the DNA molecule and provides information on the shape and volume of the complex (44,47,55). To analyze Ver binding to DNA, we made four different DNA constructs derived from the pUC18 plasmid: a construct consisting of 1260 bp of dsDNA ending in two 42-nt 3′-single-stranded overhangs (3′-double-tail construct, abbreviated with 3′-DTC); a construct consisting of 979 bp of dsDNA ending in two 42-nt 5′ single-stranded overhangs (5′-DTC), a construct containing 860 bp of dsDNA with a blunt end and a 42-nt ss 3′-overhang at the other end (3′-single-tail construct; 3′-STC); and a 694 bp blunt-ended dsDNA construct (blunt end construct, BEC) (Supplementary Table S1, Figure 2A). These constructs were incubated with histidine-tagged Ver (His–Ver), which binds ssDNA with approximately the same affinity of GST-Ver (Supplementary Figure S4). The relatively small size and charge of the histidine tail causes only a slight alteration of Ver molecular weight and properties, allowing an easy evaluation of protein/DNA complex stoichiometry. In order to stabilize DNA–protein interactions, complexes were crosslinked with glutaraldehyde.

As shown in Figure 2C, the Ver–DNA complexes are clearly visible in AFM images. To determine the localization pattern of these complexes we measured the distance between the center of each complex and the closest DNA end (L_1 in Figure 2B); this measure was obviously equal or less than half the length of the construct. Thus, to map the complexes, we considered only half of each construct, which was subdivided into consecutive sections of 10.2 nm (corresponding to approximately 30 bases). We then used L_1 to assign each complex to one of the regions into which the four DNA constructs were subdivided (Figure 3). As a positive control for our experimental set-up, we used the *Escherichia coli* SSB protein, which binds ssDNA with high affinity (Supplementary Figure S5) in a sequence-independent fashion (49,56).

An analysis of Ver–DNA complexes distribution along the four constructs revealed striking differences. These complexes were randomly distributed on BECs (Figure 3A). In contrast, 3′-STCs, 3′-DTCs and 5′-DTCs displayed strong accumulations of the complexes in the terminal regions. In the 3′-STCs, 50% of the complexes mapped to the terminal segment (Figure 3B), while 55% of the complexes were concentrated in the terminal regions of 3′-DTCs (Figure 3C). The analysis of His–Ver binding to 5′-DTCs showed that 57% of the complexes were located in the terminal segment (Figure 3D), similar to what found for the 3′-ending probe 3′-DTC. These results are in agreement with the EMSA analysis (Figure 1C) and indicate that Ver has no preference for 3′ or 5′ overhangs. Importantly, the SSB protein, which has a greater ssDNA-binding affinity than Ver, was randomly bound to BEC (Figure 3E) but preferentially associated with the ends of the STCs and DTCs just like Ver,

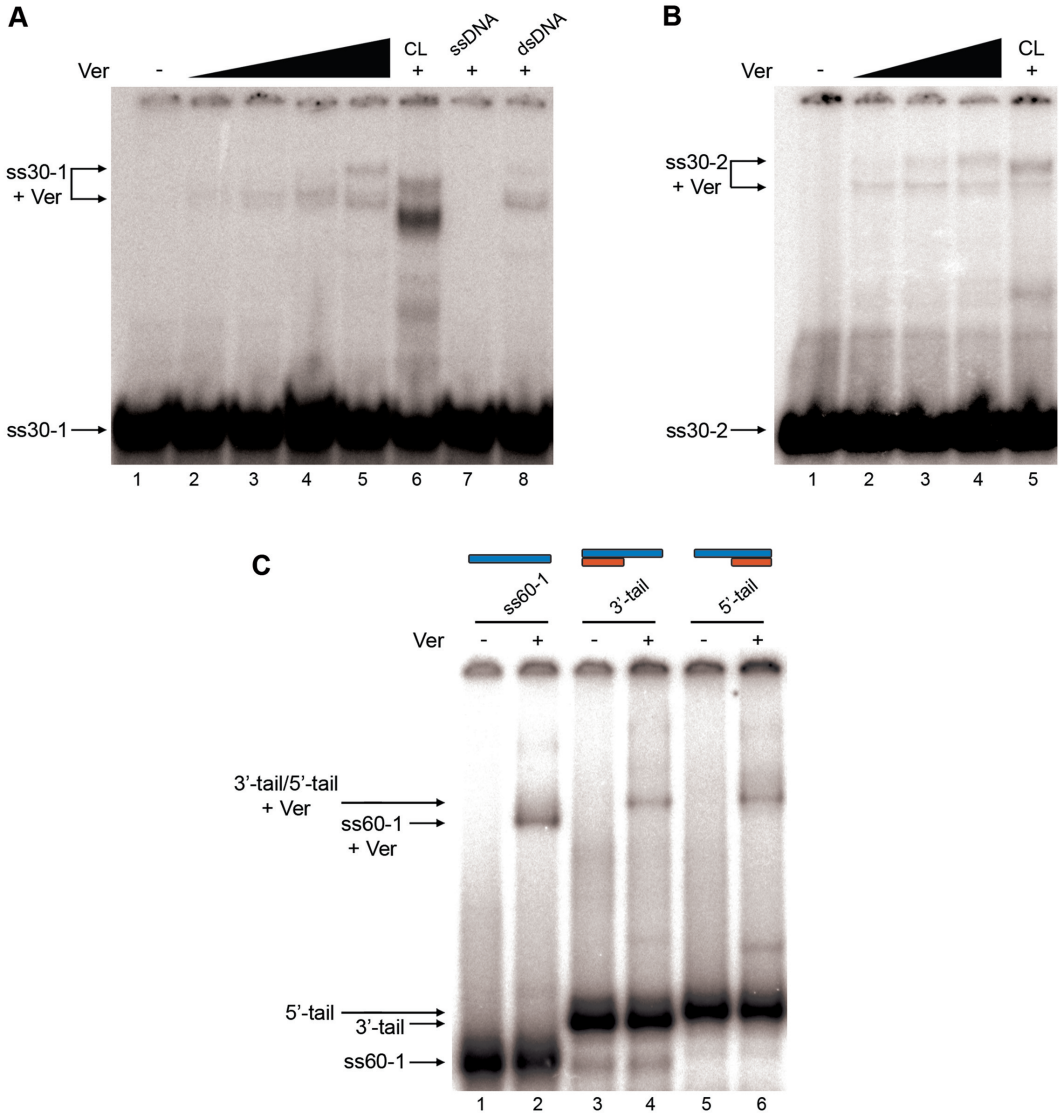

Figure 1. Ver binds ssDNA in vitro with no preference for 3′ or 5′ overhangs. (**A**) 10 nM labeled ss30-1 oligonucleotide incubated with GST-Ver at increasing concentrations and separated on 5% polyacrylamide gel. Lanes 1–5, GST-Ver concentration: 0, 11, 33, 100 and 300 nM; lane 6, 300 nM GST-Ver, complex crosslinked with 0.1% glutaraldehyde; lane 7, competition with 1 μM ss30-2 oligonucleotide; lane 8, competition with 1 μM calf thymus ds DNA. (**B**) 10 nM labeled ss30-2 oligonucleotide incubated with GST-Ver at increasing concentrations and separated on 5% polyacrylamide gel. Lanes 1–4, GST-Ver concentrations: 0, 33, 100 and 300 nM; lane 5, 300 nM GST-Ver, complex crosslinked with 0.1% glutaraldehyde. (**C**) Lanes 1–2, 10 nM labeled ss60-1 oligonucleotide; lanes 3–4, 10 nM labeled 3′-tail DNA; lanes 5–6, 10 nM labeled 5′-tail DNA. (–) no protein, (+) 100 nM GST-Ver.

with binding profiles very similar to those observed for Ver (Figure 3F–H).

We also asked whether the terminal accumulation of Ver in the 3′-STCs, 3′-DTCs and 5′DTCs reflects binding to ssDNA, which is not visible in our AFM images. We thus considered the constructs showing Ver binding at one of the extremities, and measured the L_2 distance between the inner edge of the complex and the opposite end of the construct (Figure 4, left panels). We posit that when Ver is bound at a terminal position on dsDNA, L_2 will be shorter than the contour length L of the construct, due to the DNA portion masked by the protein. In the few BECs showing Ver at their extremities the distance L_2 was indeed significantly shorter than L (Figure 4A), whereas in STCs and DTCs L_2 and L were virtually identical (Figure 4B–D). This finding strongly suggests that in STCs and DTCs, Ver is mostly bound to the overhanging ssDNA. Collectively, the results of the AFM experiments confirm and extend the conclusions derived from the EMSA experiments, indicating that Ver binds DNA with a strong preference for regions terminating with ssDNA overhangs that mimic the typical structure of eukaryotic telomeres.

Finally, we measured the volumes of Ver-containing structures in AFM images (47,57) to derive their molecular masses (57). The volumes distribution of unbound Ver showed a maximum around 70 nm^3 (Supplementary Figure S6A), which is consistent with the volume of a Ver dimer estimated by calibration with the SSB volume (Supplementary Figure S6C, see Materials and Methods for full explanation). The volume distribution of Ver bound to DNA was

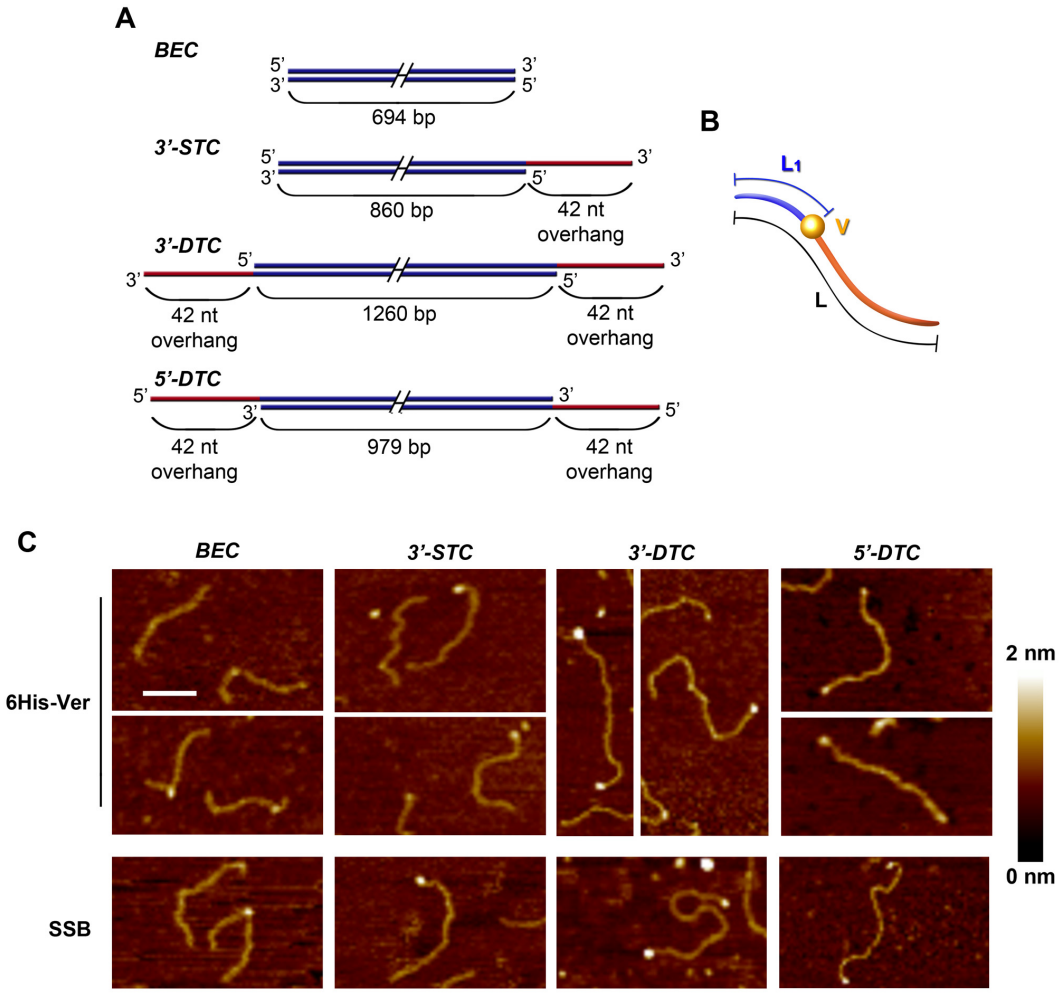

Figure 2. AFM imaging of Ver and SSB binding to blunt-ended, 3′-protruding, or 5′-protruding DNA probes. (**A**) Schematic representation of the DNA constructs used in AFM experiments. (**B**) Schematic representation of the distances measured on AFM images: L_1, distance between the center of the nucleoprotein complex and the closest end of the construct, L is the contour length of the entire construct. (**C**) Gallery of AFM images of Ver and SSB bound to the four DNA probes. Scale bar, 100 nm.

considerably broader than that of free Ver, suggesting that Ver binds ssDNA as a dimer or a multimer (Supplementary Figure S6B).

Ver contains a multimerization domain required for telomere protection

Consistent with our AFM observations, we have previously shown by GST pull-down that GST-Ver is able to bind 6His–Ver, indicating that Ver is able to multimerize (40). To identify potential Ver interacting residues involved in dimerization, we performed interface prediction using CPORT, a computational method based on five interface predictors (58). An α-helix between residues 185 and 204 is the most likely Ver dimerization domain. This α-helix spans the entire length of the OB fold and contains several solvent-exposed hydrophobic residues (Met190, Phe194, Tyr197, Trp201; see Figure 5A), suggesting that this motif may be involved in protein-protein interactions. To verify this prediction, we generated $ver^{\Delta C}$, a terminally deleted gene that encodes a Ver protein lacking aa 186–214. Differently from full-length GST-Ver, GST-$Ver^{\Delta C}$ was unable to bind 6His–Ver (Figure 5B), indicating that the Ver C-terminal domain is essential for Ver–Ver interactions.

To assess the localization of $Ver^{\Delta C}$ *in vivo* we generated transgenic flies expressing $Ver^{\Delta C}$-GFP in a ver^1 mutant background. Immunostaining of polytene chromosome nuclei with an anti-GFP antibody showed that $Ver^{\Delta C}$-GFP localizes to distinct foci that correspond to the telomeres (Figure 5C), indicating that the mutant protein is recruited at telomeres just like its wild type counterpart. However, $Ver^{\Delta C}$ is unable to ensure telomere protection, as larval brain cells from ver^1 mutants that express $Ver^{\Delta C}$ showed the same frequency of telomeric fusions as ver^1 mutants (40) (60% cells with at least one telomere fusion per cell; n = 100).

We next verified the ability of $Ver^{\Delta C}$ to bind ssDNA. EMSA experiments using purified GST-$Ver^{\Delta C}$ protein showed that $Ver^{\Delta C}$ is unable to bind ssDNA (Figure 5D). This finding suggests that the ssDNA binding activity of Ver is essential for telomere protection and supports the hy-

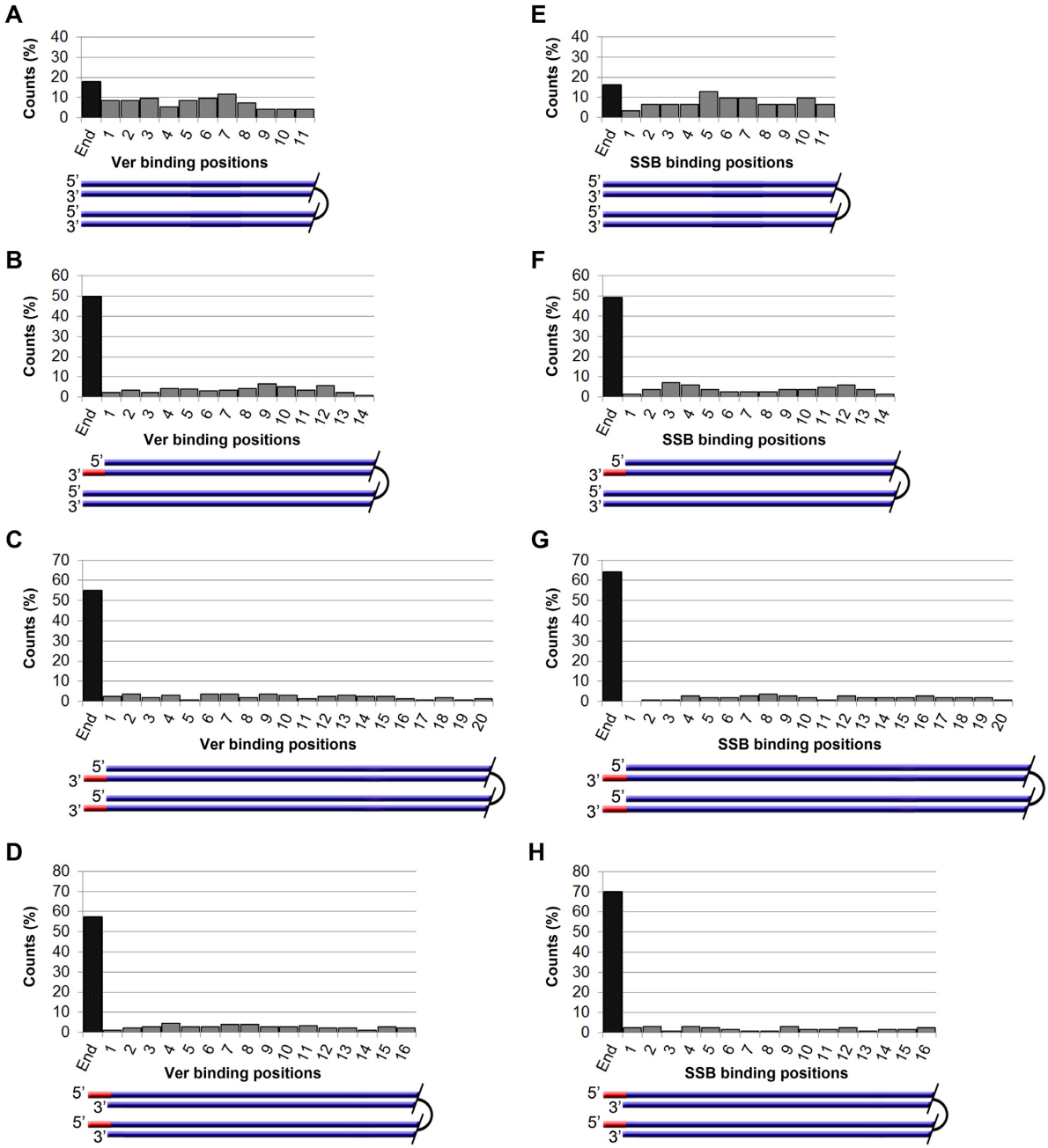

Figure 3. Analysis of Ver–DNA and of SSB-DNA complexes distribution along different DNA constructs shows that Ver preferentially binds ssDNA. (**A**) Distributions of Ver–DNA complexes along the eleven 30 bp segments that comprise half BEC. Each complex was assigned to a specific segment based on the distance between the center of the complex and the closest end of the DNA construct (L_1 in Figure 2B). Counts represent percent of bound DNA molecules ($n = 94$ bound molecules out of 314 DNA molecules counted). End indicates complexes associated with the BEC termini. (**B**) Distributions of Ver–DNA complexes along the fourteen 30 bp segments that comprise half 3′-STC ($n = 233$ bound molecules out of 425); see (A) for explanation. End includes complexes associated with either a ssDNA or a blunt terminus. (**C**) Distributions of Ver–DNA complexes along the twenty 30 bp segments that comprise half 3′-DTC ($n = 163$ bound molecules out of 218); see (A) for explanation. End includes proteins bound to both 3′-DTC termini. (**D**) Distributions of Ver–DNA complexes along the sixteen 30 bp segments that comprise half 5′-DTC ($n = 183$ bound molecules out of 324); see (A) for explanation. End includes proteins bound to both 5′-DTC termini. (E–H) Distributions of SSB-DNA complexes along (**E**) half BEC, $n = 31$ bound molecules out of 182; (**F**) half 3′-STC, $n = 85$ bound molecules out of 173; (**G**) half 3′-DTC, $n = 115$ bound molecules out of 170; (**H**) half 5′-DTC, $n = 127$ bound molecules out of 208. See legends for A–D for explanations.

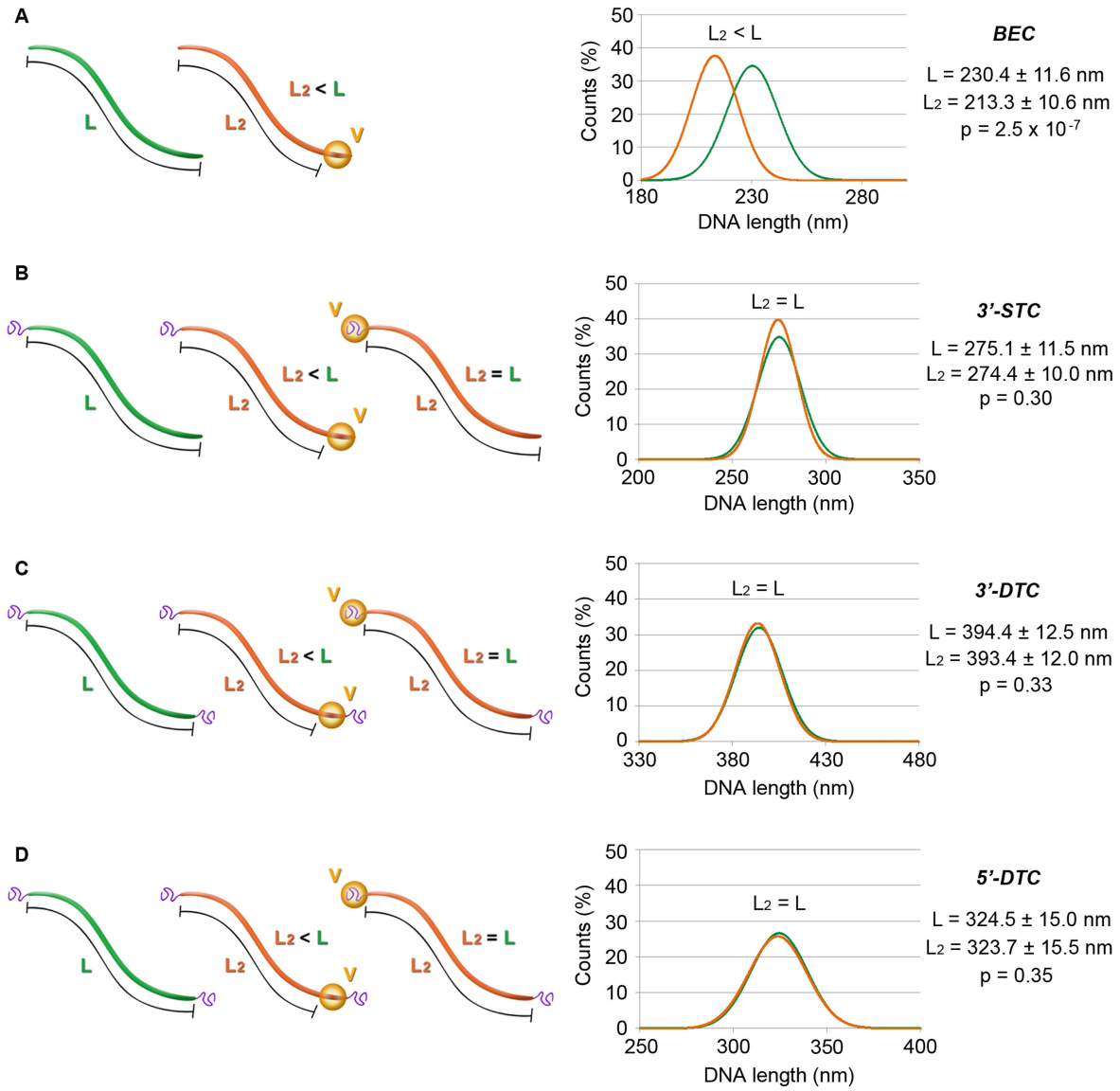

Figure 4. A comparison between the contour lengths of unbound and Ver-end-bound constructs confirms that Ver binds ssDNA overhangs. Left, schematic representation of contour lengths measured on AFM images of naked DNA and terminally-bound Ver/DNA complexes; *L* is the length of the naked DNA construct, and L_2 the distance between the edge of a bound protein and the opposite end of the construct. Right, Gaussian fitting of the distributions of L_2(orange) and *L* (green). *P* values were determined with Student's *t* test. (**A**) When Ver is bound to the end of BECs, L_2 is expected to be shorter than the contour length of naked DNA ($L_2 < L$); the Gaussian fitting of the distributions of *L2* and *L* is in agreement with this prediction. Terminally bound molecules: $n = 17$; naked DNA molecules: $n = 220$. (B–D) There are two possible expectations for 3′-STCs (**B**), 3′-DTC (**C**) and 5′-DTCs (**D**). If Ver is bound at the terminal DNA duplex, L_2 should be shorter than *L*, as in BECs. In contrast, if Ver is bound to ssDNA, L_2 should be equal to *L*. The Gaussian distributions of *L* and L_2 for both STCs and DTCs are virtually identical, supporting the conclusion that Ver binds ssDNA. Terminally bound and naked DNA molecules are 116 and 192 in (B), 90 and 55 in (C), 105 and 141 in (D), respectively.

pothesis that Ver binds telomeric ssDNA as a dimer or a multimer. However, our data do not exclude the possibility that the DNA binding and dimerization functions residing in the C-terminal part of Ver might be separate.

Moi is required for Ver localization at telomeres but not for its binding to ssDNA

Moi is a terminin component that directly interacts with both HOAP and Ver (32,39,40). However, the hypothesis that Moi and Ver form a complex is mainly based on *in vitro* studies (32,40). To ascertain whether a Moi–Ver complex exists *in vivo*, we performed GFP-TRAP-affinity purification and mass spectrometry (AP-MS) on extracts from embryos expressing Ver-GFP. We first imaged live embryos expressing Ver-GFP and verified that the protein localizes exclusively at telomeres also in embryos (Figure 6A and Movies S1 and S2). We also assayed the efficiency of our affinity purification procedure; we found that incubation with GFP-TRAP-A of clarified 1–3 h embryo extracts consistently depleted 95% of Ver-GFP (data not shown).

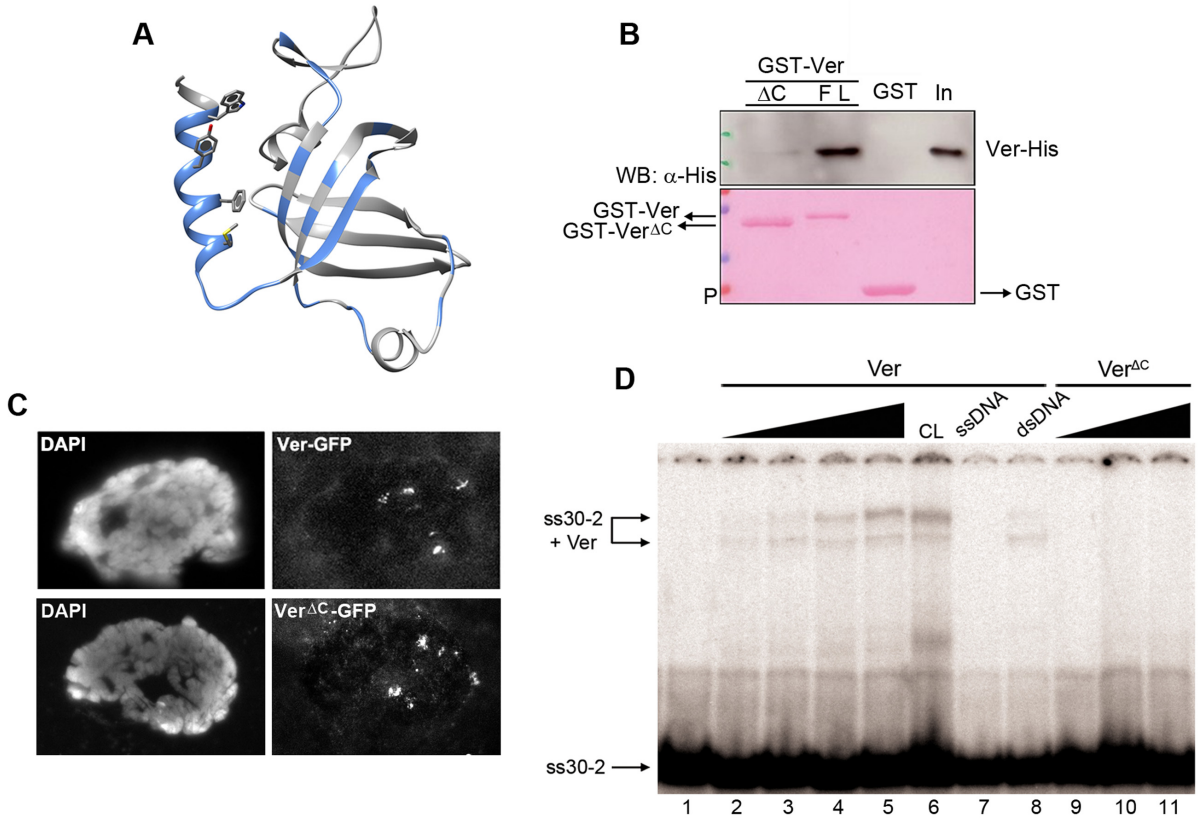

Figure 5. The Ver C-terminal domain is required for Ver multimerization and ssDNA binding. (**A**) Predicted Ver dimerization interface using CPORT. Residues involved in the interaction are colored in blue, while the exposed hydrophobic residues of the C-terminal helix are represented as sticks. (**B**) GST-pulldown assay showing that GST-Ver, but not GST-Ver$^{\Delta C}$, binds 6His–Ver. His–Ver is visualized by anti-His WB, GST-Ver by Ponceau staining (P); FL, full length Ver; In, input. (**C**) Localization of Ver-GFP and Ver$^{\Delta C}$-GFP in fixed salivary gland nuclei immunostained with anti-GFP antibodies. Note the discrete Ver signals at the telomeres. (**D**) EMSA showing that Ver$^{\Delta C}$ does not bind ssDNA. 10 nM labeled ss30-2 oligonucleotide incubated with GST-Ver or GST-Ver$^{\Delta C}$ at increasing concentrations and separated on 5% polyacrylamide gel. Lanes 1–5, GST-Ver concentrations: 0, 11, 33, 100 and 300 nM; lane 6, 300 nM GST-Ver, complexes crosslinked by treatment with 0.1% glutaraldehyde; lane 7, competition with 1 μM ss30-1 oligonucleotide; lane 8, competition with 1 μM calf thymus dsDNA; lanes 9–11, increasing GST-Ver$^{\Delta C}$ concentrations: 33, 100 and 300 nM.

Bioinformatics-based analysis of AP precipitates after stringent filtering against a previously described database of known false positives (52) identified three putative Ver interacting proteins present at quantities of 1:100 or greater relative to Ver (i.e. Area relative to bait > 0.01); Moi, the CG30007 and CG7341 proteins (Figure 6B). While CG7341 is currently uncharacterized, CG30007 has been recently shown to be required for telomere protection from fusion events and has been named Tea (59). Collectively, these results strongly suggest that Moi, Ver and Tea form a complex *in vivo*.

The strong biochemical interaction between Ver and Moi, and their mutual dependency for telomere localization raises the question of whether they cooperate for ssDNA binding. To address this question, we first performed EMSA after incubation of GST-Moi with the ss30-1 oligo and did not detect any DNA–Moi complex (Figure 7A). We then analyzed GST-Ver binding to the same oligo in the presence of GST-Moi and did not see any variation from the DNA binding pattern observed after incubation with GST-Ver alone (Figure 7B). These results indicate that Moi is unable to bind ssDNA on its own and that the presence of Moi does not affect Ver binding to DNA.

Ver-depleted telomeres elicit DNA damage response

The finding that Ver binds ssDNA raises the possibility that upon depletion of Ver, this ssDNA might become unprotected, eliciting DNA damage response (DDR). In mammalian cells, failure to recruit POT1 at the telomeres leads to the accumulation of RPA and γ-H2AX at chromosome ends and to a robust DDR (13–17,60). To determine whether *Drosophila* telomeres are recognized as sites of DNA damage in the absence of Ver, we immunostained salivary gland polytene chromosomes of wild type and *ver* mutants with an antibody specific for the phosphorylated form of *Drosophila* H2AX (γ-H2AV) (61) and for the telomere-specific marker HOAP (Figure 8A). In wild type, we detected γ-H2AV signals at the chromocenter, along the euchromatic arms, and at 47% of the telomeres ($n = 157$); similar results were previously obtained using a different anti-γ-H2AV antibody (62). In 94% of the telomeres labeled with γ-H2AV the signal was smaller or coincident with the HOAP signals (γ-H2AV≤HOAP, henceforth weak γ-H2AV signal) and only in 6% of these telomeres the γ-H2AV signal was larger than the HOAP signal (γ-H2AV>HOAP, henceforth strong γ-H2AV signal (Figure 8B); a quantification of the ratios between γ-H2AV

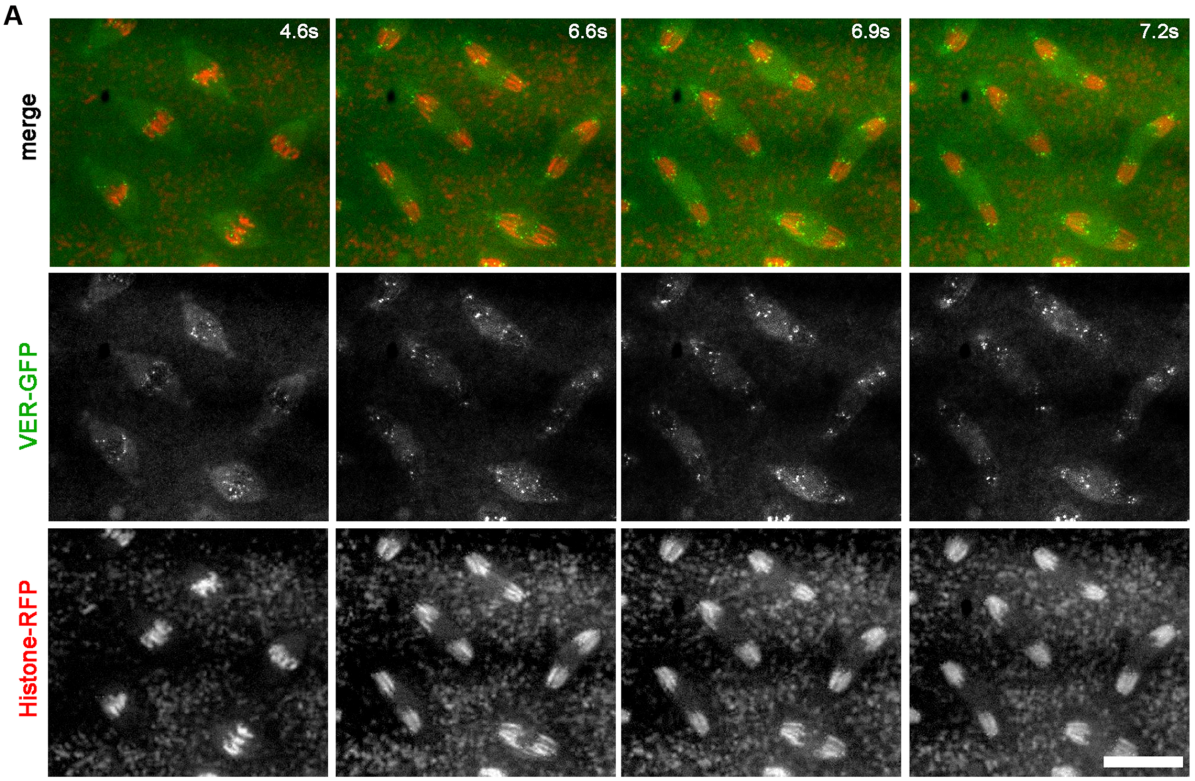

B

Protein name	Protein ID	Percentage Coverage	Number of Peptides	MW [kDa]	Score	Area	Area relative to BAIT
Verrocchio	FBpp0304177	51.87	9	24.4	888.27	13,599,845,600	1.00
Modigliani	FBpp0289215	35.39	7	20.2	111.79	1,217,705,602	0.09
CG30007	FBpp0290141/43	24.73	34	211.7	298.19	826,139,608	0.06
CG7341	FBpp0074889	30.53	8	41.1	66.44	74,887,895	0.01

Figure 6. Ver, Moi and CG30007 form a complex in *Drosophila* embryos. (**A**) Stills from a time-lapse video of an embryo expressing Ver-GFP (green) and Histone-RFP (red), showing that Ver-GFP is specifically localized at telomeres. Time in each frame is given in seconds from the start of imaging. Images show two separate groups of telomeres moving to the spindle poles; the telomeres closer to the poles are those of the dot (fourth) chromosomes and the short arm of the acrocentric X chromosome. These telomeres are very close to the centromeres and are therefore expected to be located near the poles of the anaphase figures. Scale bar: 10 μm. (**B**) Proteins identified via mass spectrometry isolated from 0 to 3 h Ver-GFP expressing *Drosophila* embryo extracts after stringent filtering (see Materials and methods). The proteins shown have MS scores >50 and coverage percentages >20%, respectively. The mean area corresponds to Top 3 Protein Quantification (T3PQ), the mean of the three highest abundance peptides identified for each protein (area relative to bait >0.01). AP identified Moi as the interactor of highest abundance (~10-fold less than the bait protein). In addition, a novel interacting protein, CG30007, was identified as the protein of next-highest abundance.

and HOAP signals is shown in Figure 8C). In *ver* mutants, we did not observe a significant increase in the frequency of γ-H2AV-labeled telomeres (47%; $n = 110$) compared to wild type. However, the frequency of telomeres displaying a strong γ-H2AV signal was significantly increased compared to control; 54% of the γ-H2AV-labeled telomeres displayed weak signals, while the remaining 46% were associated with very strong signals. Consistent with these results, 48% ($n = 170$) of the polytene chromosome telomeres of *moi* mutants showed γ-H2AV signals, which were weak in 47% of the telomeres and strong in the remaining 53% (Figure 8B). Thus, γ-H2AV associates with both wild type and Ver-deficient telomeres, but the accumulation of this DDR marker was greater at *ver* mutant telomeres than at their wild type counterparts.

Previous studies showed that human and mouse chromosomes exhibit γ-H2AX signals at telomeres, and that the frequency of these signals is increased either by prolonged metaphase arrest or loss of telomere protection factors (63,64). Thus, we asked whether the mitotic chromosomes of *ver* mutants accumulate γ-H2AV foci at chromosome ends. Immunostaining of wild type metaphases ($n = 100$) with anti- γ-H2AV antibodies showed an irregular and rather diffuse staining of the chromosomes without clear γ-H2AV accumulations at the telomeres. In contrast, metaphases ($n = 200$) of *ver* mutants displayed strong telomeric accumulations of γ-H2AV, with an average of 2.5 telomere-associated foci per cell (Figure 8D). Thus, γ-H2AV appears to be substantially enriched at Ver-depleted telomeres, while no clear γ-H2AV foci were detectable at wild type telomeres.

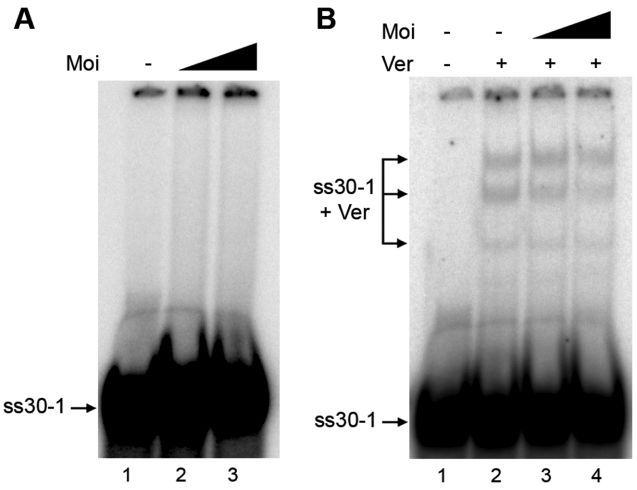

Figure 7. Moi neither binds ssDNA nor is needed for Ver binding to ssDNA. (**A**) EMSA showing that GST-Moi does not bind single-stranded DNA. 10 nM labeled ss30-1 oligonucleotide was incubated with increasing concentrations of GST-Moi and separated on 5% polyacrylamide gel. Lane 1, no protein; lanes 2 and 3, 100 and 400 nM GST-Moi. (**B**) EMSA showing that GST-Moi does not affect binding of GST-Ver to ssDNA. 10 nM labeled ss30-1 oligonucleotide was incubated with 300 nM GST-Ver (lanes 2–4) and increasing concentrations of GST-Moi, and separated on 5% polyacrylamide gel. Lane 1, no protein; lanes 3 and 4, 100 and 400 nM GST-Moi.

Telomere-associated γ-H2AX foci have been observed in unperturbed chromosomes of both yeast and mammalian cells, and they are thought to reflect transient telomere deprotection events resulting in persistent accumulation of γ-H2AX (63–65). The presence of relatively small γ-H2AV foci at 50% of the wild type polytene telomeres suggests that *Drosophila* telomeres behave like those of yeast and mammals. However, clear foci were not seen at the ends of wild type mitotic chromosomes. Although this finding might reflect structural differences between mitotic and polytene chromosome telomeres, we believe it is instead a consequence of the lateral multiplicity of polytene chromosomes ends, which allows visualization of γ-H2AV amounts that would be below the detection level in mitotic chromosomes. However, both mitotic and polytene chromosomes of *ver* mutants displayed large γ-H2AV foci at their ends, indicating that Ver protects both types of telomeres from DDR.

It has been previously shown that in POT1-depleted cells replication protein A (RPA) accumulates at telomeres and recruits ATR that signals DNA damage (16,66). We thus asked whether Ver-depleted telomeres bind the RPA complex. We generated flies that ubiquitously express the large RPA subunit (RPA-70) fused to GFP (GFP-RPA70) in either a wild type or a *ver* mutant background. Co-immunostaining of polytene chromosomes with anti-GFP and anti-γ-H2AV antibodies detected a GFP signal on 10% of the wild type telomeres ($n = 80$); 75% of these RPA-associated telomeres also showed a γ-H2AV signal (Figure 9B). In *ver* mutants, 49% of the telomeres ($n = 131$) displayed a clear GFP-RPA70 signal, and most of these telomeres (95%) also showed a strong γ-H2AV signal (Figure 9A and B). These results indicate that loss of Ver strongly increases RPA and γ-H2AV recruitment at *Drosophila* telomeres.

Ver physically interacts with RPA70

Studies on mammalian cells have shown that telomeres bind RPA during DNA replication, and that RPA is replaced by specialized ssDNA-binding telomere proteins, such as POT1, at the end of DNA replication (60,67). Therefore, to protect their telomeres, cells must dislodge RPA from chromosome ends, so as to favor binding of telomere capping proteins. This protein switch is likely to occur in a window of time when RPA and the telomeric ssDNA binding protein are simultaneously present at telomeres. Consistent with this idea, in budding yeast RPA physically interacts with the Cdc13 protein that binds the telomeric ssDNA overhang (68). Thus, Ver and RPA might physically interact at *Drosophila* telomeres. To test this possibility we performed Co-IP experiments on S2 cell lines expressing RPA70-FLAG and GFP-Ver. IP with anti-FLAG antibodies precipitated GFP-Ver from extracts expressing both RPA70-FLAG and GFP-Ver but not from extracts expressing GFP-Ver alone (Figure 9C). In the reciprocal experiment, anti-GFP antibodies precipitated RPA70-FLAG from extracts expressing both tagged proteins but not from extract containing RPA70-FLAG alone (Figure 9D). Notably, the GFP-Ver/RPA70-FLAG interaction was observed both in the presence and in the absence of DNase I, suggesting that it is mediated by contacts between proteins.

DISCUSSION

Ver binds telomeric single-stranded DNA

We have previously shown that the integrity of the Ver OB-fold domain is dispensable for Ver recruitment at telomeres but is crucial for telomere protection from fusion events. These results suggested but did not prove that Ver possesses ssDNA binding activity (40). Here we provide strong evidence that Ver binds ssDNA. EMSA experiments showed that Ver-GST binds ssDNA probes of different sequence, and that this binding is reduced by competition with ssDNA but not dsDNA. In addition, our AFM experiments unambiguously showed that Ver binds DNA with a strong preference for the terminal regions of DNA molecules that end with either 3′ or 5′ ssDNA overhangs. Collectively, both the results of our experiments and previous studies on *Drosophila* telomeres (reviewed in (32,38,69)) strongly suggest that Ver binds ssDNA in a sequence-independent manner. However, we cannot exclude that diverse DNA sequences could bind Ver with different affinities.

We have also shown that Ver binds ssDNA as a dimer or a multimer. We mapped the protein domain required for Ver–Ver interaction and showed that in the absence of this domain Ver is unable to bind ssDNA and to protect telomeres from fusion events, providing additional evidence that the Ver capping function relies on intact ssDNA binding activity. The presence of ssDNA at *Drosophila* telomeres has never been directly demonstrated, as the variability of fly telomeric DNA prevented successful application of the commonly used DNA sequence-based methods to

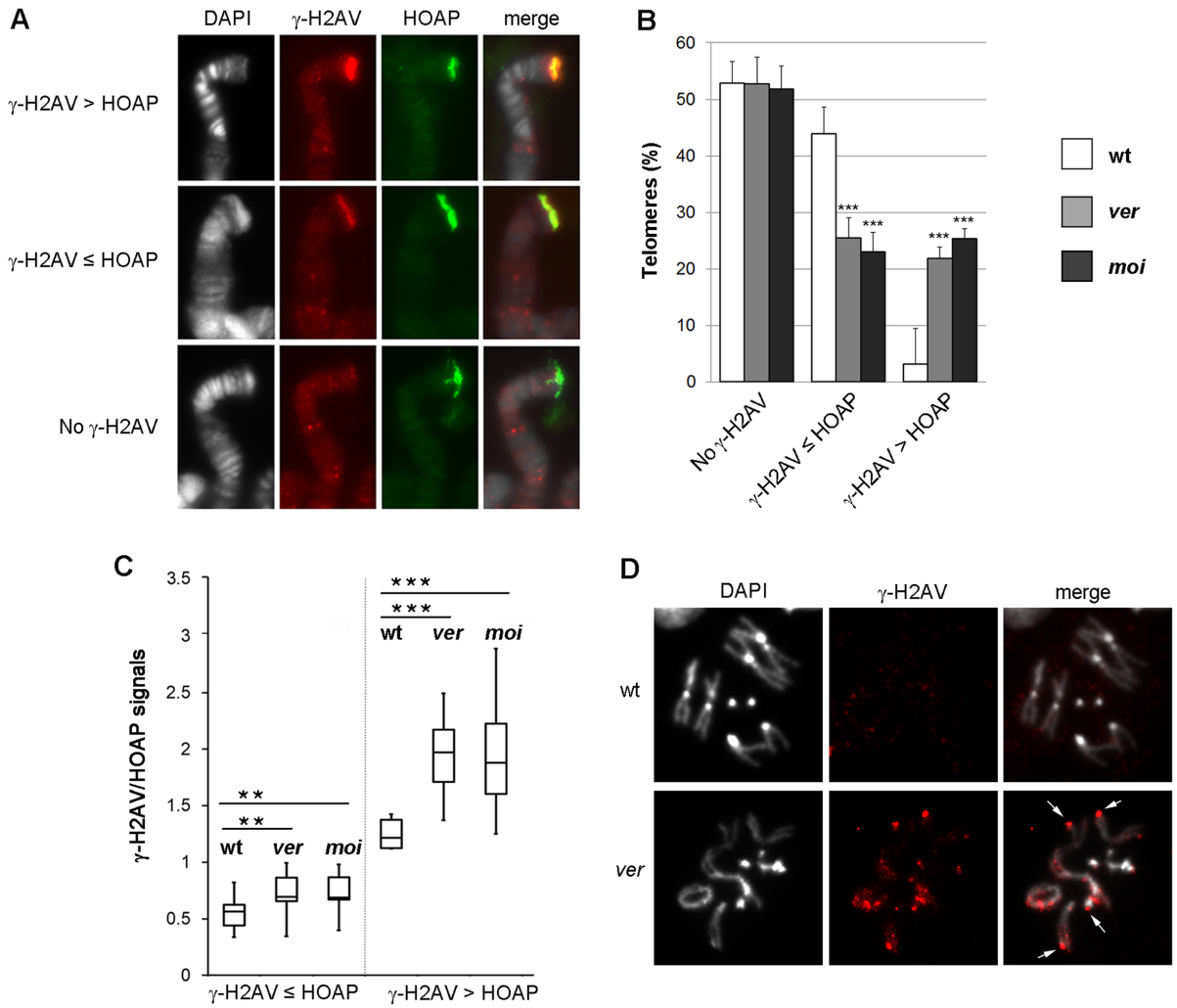

Figure 8. Telomeres of *ver* and *moi* mutants exhibit prominent γ-H2AV signals. (A, B) γ-H2AV signals at polytene chromosome telomeres stained for both γ-H2AV and HOAP. (**A**) Examples of HOAP-stained (green) telomeres displaying no γ-H2AV signal, or γ-H2AV signals (red) weaker/equal (≤) or stronger (>) than the HOAP signal. The fluorescence intensities of the signals were determined using the ImageJ software; see Materials and methods for details. (**B**) Frequencies (± SEM) of telomeres showing the types of γ-H2AV/HOAP signals illustrated in (A); the frequencies of signals with γ-H2AV> HOAP observed in *moi* and *ver* mutants are significantly higher (***$P < 0.001$, Mann–Whitney test) than those seen in controls (wt). (**C**) Box plot representation of the distribution of the ratios between the γ-H2AV and the HOAP signal intensities, relative to the histograms shown in B. The lines inside the box plot indicate the medians of the ratios observed in each genotype; the box boundaries represent the upper and lower quartiles, whiskers indicate 1.5 interquartile ranges. **$P < 0.01$; ***$P < 0.001$ (Student's *t* test). (**D**) Formation of prominent γ-H2AV foci at the mitotic chromosome telomeres (arrows) of brain cells from *ver* mutant larvae. Note the irregular and rather diffuse distribution of γ-H2AV on wild type chromosomes.

characterize the structure of chromosome ends. The findings that Ver binds ssDNA and is required for telomere capping strongly suggests that fly telomeres do in fact terminate with a ssDNA like those of yeasts, plants, and mammals. Studies on *C. elegans* have shown that this species possesses both 3′ and 5′ overhangs that are bound by 2 different proteins, CeOB1 and CeOB2, which exhibit specificity for G-rich or C-rich telomeric overhangs, respectively (19). Our data would suggest that Ver could bind both 5′ and 3′ overhangs. However, they do not prove that these overhangs coexist in living flies.

Our results indicate that Ver binds ssDNA with low affinity, as even high protein concentrations were not sufficient to significantly reduce the amount of unbound probe. However, in a very recent study, Zhang *et al*. showed that a trimeric complex formed by recombinant Tea, Moi and Ver, purified with the baculovirus system, has robust sequence independent ssDNA binding activity, while a Moi–Ver subcomplex is unable to bind ssDNA (59). We believe that the results of our work and those of Zhang and coworkers (59) are not contradictory and integrate with each other. Their failure to detect interactions between the Moi–Ver subcomplex and ssDNA is probably due to the protein tags and purification methods they used. On the other hand, they clearly showed that Moi, Tea and Ver have high ssDNA binding activity when they act as a trimeric complex. Tea has not obvious ssDNA binding motifs, and remains to be determined whether Tea has its own ssDNA binding activity or simply enhances Ver binding activity.

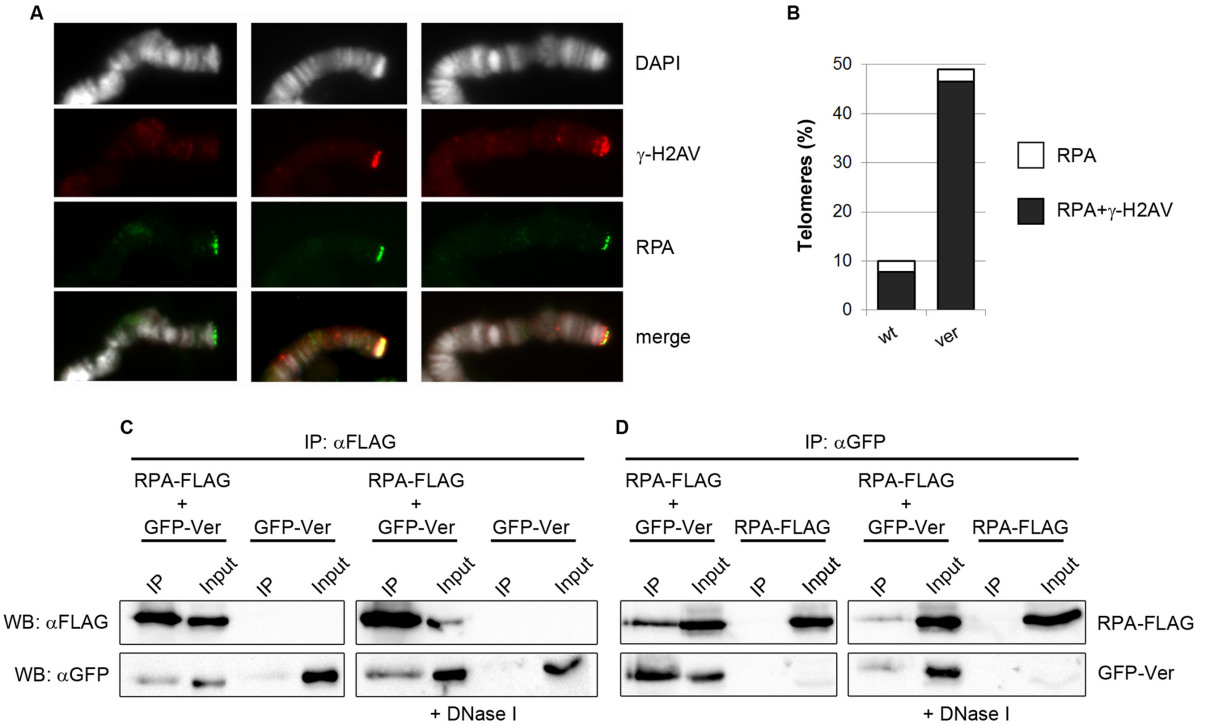

Figure 9. GFP-RPA is enriched at Ver mutant telomeres and physically interacts with Ver. (**A**) Polytene chromosomes from *ver* mutant larvae bearing a UAS-GFP-RPA transgene and an actin-GAL4 driver co-immunostained with anti-GFP (green) and anti-γ-H2AV (red) antibodies. A few telomeres exhibit a GFP-RPA signal only (left panels), while most telomeres show overlapping GFP-RPA and γ-H2AV signals (central and right panels). (**B**) Frequencies of telomeres associated with GFP-RPA only or with both GFP-RPA and γ-H2AV in wt or *ver* mutant larvae. The frequency of GFP-RPA/γ-H2AV labeled telomeres observed in *ver* mutants is significantly higher than that seen in wild type ($P < 0.0001$; Mann-Whitney test). (C, D): Physical interaction between RPA and Ver. Co-IPs were performed with anti-FLAG (**C**) or anti-GFP antibodies (**D**) using extracts from S2 cells expressing the indicated tagged proteins. The RPA-Ver interaction is not affected by a pre-treatment of extracts with DNaseI (right panels in C and D).

The low ssDNA binding affinity of the Ver protein is likely to reflect specific functional requirements. For example, it is conceivable that Ver low affinity for ssDNA prevents unwanted binding of Ver to other ssDNA regions such as those formed during normal DNA replication. It should be noted that telomeric proteins that bind ssDNA with relatively low affinity independently of the sequence have been previously described in yeasts and mammals. For example, Pot1 of *S. pombe* possesses an N-terminal OB fold that binds DNA in a sequence-dependent fashion, and a C-terminal OB fold with sequence-independent binding properties, a feature that is likely to reflect the need to protect the degenerate telomere sequences present in this yeast species (70). Another ssDNA binding protein that exhibits no preference for telomeric substrates is *C. albicans* Cdc13. As a consequence, while *S. cerevisiae* Cdc13 is recruited at telomeres through sequence-specific interaction with telomeric DNA, recruitment of *C. albicans* Cdc13 relies on protein-protein interactions (71). Remarkably, also a high-affinity ssDNA binding complex such as TPP1-POT1 is recruited at telomeres by TIN2, which bridges these ssDNA binding proteins to the dsDNA binding proteins TRF1 and TRF2 (17). Most likely, also Ver recruitment at telomeres depends on interactions with other terminin components and not with telomeric DNA. This is suggested by the behavior of $Ver^{\Delta C}$. Although this truncated Ver moiety fails to bind ssDNA and to prevent end-to-end fusions, it is normally recruited at telomeres.

We have previously shown that Ver and Moi are both mutually dependent and HOAP dependent for their localization at telomeres (39,40); HOAP binds dsDNA (72) and coats up to 10 kb of telomeric DNA (42). These findings suggested that HOAP could mediate Ver and Moi recruitment at telomeres (39,40). However, recent work has shown that Moi and Ver association with telomeres is also dependent on Tea, which requires HOAP for its telomeric localization (59). Because HOAP localizes normally at telomeres in *tea* mutants (59), these findings suggest that Tea, in the presence of HOAP, could mediate Ver and Moi recruitment at telomeres.

Ver prevents DNA damage signaling at telomeres

Although the pathways leading to end-to-end fusion in *Drosophila* have not been fully elucidated, this study has provided evidence that the early steps of telomere dysfunction recognition are conserved between mammals and flies. We have indeed shown that fly telomeres depleted of Ver-Moi accumulate RPA and γ-H2AV just as mammalian telomeres lacking TPP1-POT1 (13–17). It is likely that in the absence of Ver–Moi the telomeric ssDNA binds RPA, which is known to bind ssDNA with high affinity (73); RPA is then likely to recruit the DNA repair machinery that leads to the formation of telomere associated γ-H2AV foci (66).

Several studies in mammalian cells have shown that following POT1 or TPP1-POT1 depletion RPA is recruited at telomeres, leading to the model that loss of POT1 unmasks the single-stranded G overhang, which binds RPA and ATR, eliciting the DDR response (14–17,60). However, it has been recently shown that POT1 is also required for proper telomere replication, probably acting in in the same pathway as CST (74). These latter findings raise the possibility that RPA localization to POT1-depleted mammalian telomeres is at least in part due to a defect in telomeric DNA replication. Our data do not allow us to exclude that Ver depletion affects telomeric DNA replication in *Drosophila*. Thus, RPA and γ-H2AV recruitment at *ver* mutant telomeres could be the consequence of an exposure of the telomeric overhang, a defect in subtelomeric/telomeric DNA replication, or both.

An interesting issue is how can the ssDNA overhangs of *Drosophila* telomeres bind Ver in a sequence independent manner and avoid binding by RPA, which has a very strong affinity for ssDNA of any sequence. In human cells, POT1 is less abundant than RPA and, although it specifically recognizes the telomeric DNA sequence (75), it binds ssDNA with lower affinity than RPA (17). Nevertheless, after each round of replication, POT1 efficiently replaces RPA at the telomere. The precise mechanism governing this protein switch has not been fully elucidated. It has been proposed that TPP1-POT1 can outcompete RPA when bound to TIN2 (17). An alternative model for the RPA-to-POT1 switch involves TERRA and the heterogeneous nuclear ribonucleoprotein A1 (hnRNPA1), which has an RPA displacing activity. It has been suggested that the low TERRA levels during the late S phase favor the hnRNPA1 activity promoting the RPA replacement with POT1 (60,67). How can Ver replace RPA at the end of DNA replication? This process might be related to dynamic transformations of the Moi–Tea–Ver complex that could modulate its affinity for ssDNA. It is also possible that the physical interaction between RPA and Ver lowers the affinity of RPA for DNA, thus allowing Ver to outcompete RPA for ssDNA binding. However, the precise mechanism governing RPA to Ver switch is currently unknown and will be a goal of our future studies.

A model for *Drosophila* terminin

In all organisms studied so far, specialized OB-fold proteins bind telomeric single stranded overhangs ensuring protection of chromosome ends. Our past and current findings on Ver broaden the list of these OB fold proteins, and strengthen the concept that the general architecture of telomere complexes is conserved across evolution, despite a remarkable plasticity in the individual components of the complexes (76–79) (Figure 10). TRF1 and TRF2 shelterin components bind the DNA duplex and are connected to the ssDNA binding protein POT1 by the non-DNA-binding TIN2 and TPP1; the shelterin-like fission yeast capping complex has similar features. It has been suggested that these shelterin complexes are functionally equivalent to the CST and Rap1–Rif1–Rif2 complexes of budding yeast (78,80) (Figure 10).

The finding that Ver but not Moi binds ssDNA suggests that terminin and shelterin have similar molecular architectures. *Drosophila* HOAP and HipHop interact with each other and are mutually dependent for their stability. In addition, ChIP analysis has shown that the two proteins are enriched over the terminal 10 kb of the chromosomes (42). Thus, even if HipHop binding to DNA has never been directly demonstrated, it is likely that the HOAP–HipHop subcomplex binds the DNA duplex. Moi binds both HOAP and Ver, and thus is likely to bridge dsDNA-binding HOAP–HipHop with ssDNA-binding Ver. Our AP/MS experiments have shown that Moi and CG30007 (Tea) are the most abundant Ver-interacting proteins, suggesting a functionally relevant interaction between the three proteins. Tea does not contain any known DNA binding domain and its DNA binding properties have not so far been investigated. Should Tea fail to bind DNA, then the structural similarity between shelterin and terminin would be even greater than that depicted in Figure 10. In both complexes, there would be a pair of proteins (TRF1–TRF2 and HOAP–HipHop) that bind the DNA duplex, a single ssDNA binding factor (POT1 and Ver) and two non-DNA-binding proteins (TIN2-TPP1 and Moi-Tea) connecting the dsDNA- and ssDNA-binding subcomplexes. Thus, although the shelterin and terminin components do not share any sequence homology, they form multi-protein complexes with similar molecular architectures.

Evolution of *Drosophila* telomere proteins

We have previously proposed that concomitant with telomerase loss *Drosophila* rapidly evolved terminin, a telomere-specific protein complex that binds and protects chromosome ends independently of their DNA sequence. We also proposed that *Drosophila* non-terminin telomere-capping proteins correspond to ancestral telomere-associated proteins that could not evolve as rapidly as terminin because of the functional constraints imposed by their involvement in diverse cellular processes (32,39,40). This hypothesis is supported by the fact that the many non-terminin proteins required for telomere capping (HP1a, ATM, Rad50, Mre11 and Nbs) have homologues playing roles at human and yeast telomeres. Additional support for this hypothesis has been provided by our recent findings on separase and pendolino/AKTIP. The conserved protease separase has been shown to be required for telomere protection in both *Drosophila* and humans (81). Pendolino (peo) prevents telomeric fusions in flies (82) while its human homologue AKTIP is required for telomere replication (83). Strikingly, Peo and AKTIP directly bind unrelated terminin and shelterin components, indicating that they co-evolved with divergent capping complexes to maintain an interaction with telomeres (82,83).

Our results on Ver provide two important additional pieces of information on the evolution of *Drosophila* telomeres. First, our findings indicate that the terminin proteins (HOAP, HipHop, Moi, Ver and possibly Tea), although fast-evolving and non conserved outside the *Drosophilidae* family, are likely to form a telomere-capping complex that is architecturally similar to the shelterin complex. Second, we have shown that *Drosophila* telomeres are likely to ter-

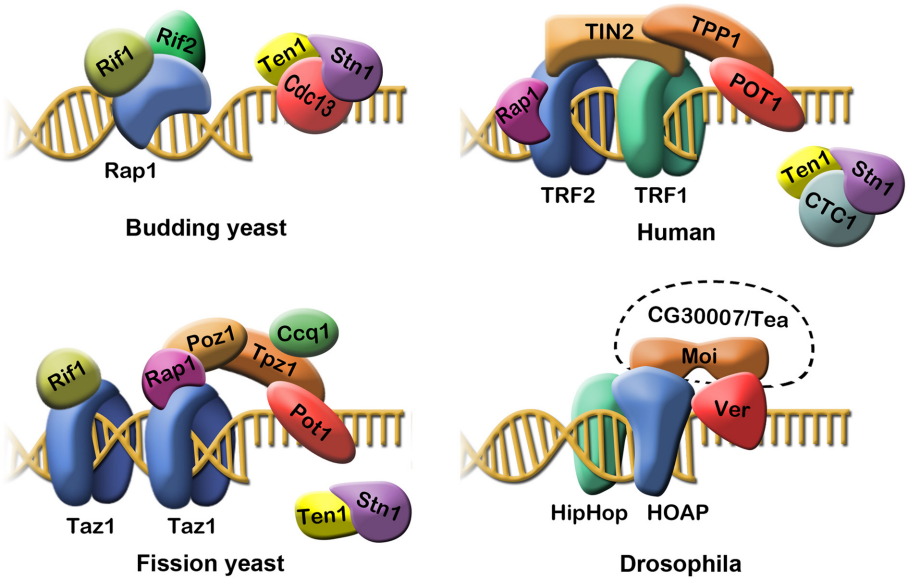

Figure 10. The telomere-capping complexes of yeast, mammals and *Drosophila* share similar molecular architectures. The human shelterin and the fission yeast shelterin-like complexes have similar architectural features. In both complexes, the proteins that bind the DNA duplex (TRF1–TRF2 and Taz1) are connected to the ssDNA-binding protein POT1 by non-DNA-binding proteins (TIN2-TPP1 and Poz1-Tpz1). Similarly, in *Drosophila* terminin, HOAP–HipHop, which bind the DNA duplex, are bridged to the ssDNA-binding Ver by Moi, which does not bind DNA. Tea directly binds Ver and Moi but it is currently unknown whether it binds DNA. It has been suggested that the POT1–TIN2–TPP1 and Pot1–Poz1–Tpz1 subcomplexes are functionally equivalent to the CST complex of budding yeast, which binds ssDNA through its Cdc13 subunit, while the Rap1–Rif1–Rif2 complex binds the DNA duplex (see text for detailed explanation and references).

minate in ssDNA overhangs that recruit RPA just like the yeast and human telomeres. Moreover, like in human telomeres, the levels of telomere-associated RPA and γH2AV (γH2AX) substantially increase when telomeres are depleted of proteins that bind the terminal ssDNA. Collectively, these results reinforce our idea that apart the capping complexes and the mechanisms of telomere length maintenance, *Drosophila* telomeres are not as different from human telomeres as generally thought (41). We thus believe that *Drosophila* is an excellent model system for studies on telomere organization and function, which can also be exploited for the identification of novel human proteins involved in telomere maintenance.

SUPPLEMENTARY DATA

Supplementary Data are available at NAR Online.

ACKNOWLEDGEMENTS

We thank Maria Grazia Giansanti for sharing reagents and Sabrina Pisano for helpful discussion and technical advice on AFM microscopy.

FUNDING

Istituto Pasteur Italia-Fondazione Cenci Bolognetti (to G.C., S.C. and G.D.R.); Agenzia Spaziale Italiana [CUP F11J11000010001 to S.C.]; Telethon [GPP13147 to G.D.R.]; Associazione Italiana per la Ricerca sul Cancro (AIRC) [IG12749 to G.C. and IG16020 to M.G.]; BBSRC grant [BB/K017837/1 to A.C.G., awarded to J.G.W.]. Funding for open access charge: Istituto Pasteur Italia – Fondazione Cenci Bolognetti.

Conflict of interest statement. None declared.

REFERENCES

1. Greider,C.W. (1996) Telomere length regulation. *Annu. Rev. Biochem.*, **65**, 337–365.
2. Hockemeyer,D. and Collins,K. (2015) Control of telomerase action at human telomeres. *Nat. Struct. Mol. Biol.*, **22**, 848–852.
3. McElligott,R. and Wellinger,R.J. (1997) The terminal DNA structure of mammalian chromosomes. *EMBO J.*, **16**, 3705–3714.
4. Zhao,Y., Sfeir,A.J., Zou,Y., Buseman,C.M., Chow,T.T., Shay,J.W. and Wright,W.E. (2009) Telomere extension occurs at most chromosome ends and is uncoupled from fill-in in human cancer cells. *Cell*, **138**, 463–475.
5. Wu,P., Takai,H. and de Lange,T. (2012) Telomeric 3' overhangs derive from resection by Exo1 and Apollo and Fill-In by POT1b-Associated CST. *Cell*, **150**, 39–52.
6. Jain,D. and Cooper,J.P. (2010) Telomeric strategies: means to an end. *Annu. Rev. Genet.*, **44**, 243–269.
7. Palm,W. and de Lange,T. (2008) How shelterin protects mammalian telomeres. *Annu. Rev. Genet.*, **42**, 301–334.
8. Ye,J., Renault,V.M., Jamet,K. and Gilson,E. (2014) Transcriptional outcome of telomere signalling. *Nat. Rev. Genet.*, **15**, 491–503.
9. Kabir,S., Hockemeyer,D. and de Lange,T. (2014) TALEN gene knockouts reveal no requirement for the conserved human shelterin protein Rap1 in telomere protection and length regulation. *Cell Rep.*, **9**, 1273–1280.
10. Sfeir,A. and de Lange,T. (2012) Removal of shelterin reveals the telomere end ion problem. *Science*, **336**, 593–597.
11. Doksani,Y. and de Lange,T. (2014) The role of double-strand break repair pathways at functional and dysfunctional telomeres. *Cold Spring Harb. Perspect. Biol.*, **6**, a016576.
12. Arnoult,N. and Karlseder,J. (2015) Complex interactions between the DNA-damage response and mammalian telomeres. *Nat. Struct. Mol. Biol.*, **22**, 859–866.
13. Wu,L., Multani,A.S., He,H., Cosme-Blanco,W., Deng,Y., Deng,J.M., Bachilo,O., Pathak,S., Tahara,H., Bailey,S.M. *et al.* (2006) Pot1 deficiency initiates DNA damage checkpoint activation and aberrant homologous recombination at telomeres. *Cell*, **126**, 49–62.

14. Denchi,E.L. and de Lange,T. (2007) Protection of telomeres through independent control of ATM and ATR by TRF2 and POT1. *Nature*, **448**, 1068–1071.
15. Barrientos,K.S., Kendellen,M.F., Freibaum,B.D., Armbruster,B.N., Etheridge,K.T. and Counter,C.M. (2008) Distinct functions of POT1 at telomeres. *Mol. Cell. Biol.*, **28**, 5251–5264.
16. Gong,Y. and de Lange,T. (2010) A Shld1-controlled POT1a provides support for repression of ATR signaling at telomeres through RPA exclusion. *Mol. Cell*, **40**, 377–387.
17. Takai,K.K., Kibe,T., Donigian,J.R., Frescas,D. and de Lange,T. (2011) Telomere protection by TPP1/POT1 requires tethering to TIN2. *Mol. Cell*, **44**, 647–659.
18. Verdun,R.E., Crabbe,L., Haggblom,C. and Karlseder,J. (2005) Functional human telomeres are recognized as DNA damage in G2 of the cell cycle. *Mol. Cell*, **20**, 551–561.
19. Raices,M., Verdun,R.E., Compton,S.A., Haggblom,C.I., Griffith,J.D., Dillin,A. and Karlseder,J. (2008) C. elegans telomeres contain G-strand and C-strand overhangs that are bound by distinct proteins. *Cell*, **132**, 745–757.
20. Kazda,A., Zellinger,B., Rossler,M., Derboven,E., Kusenda,B. and Riha,K. (2012) Chromosome end protection by blunt-ended telomeres. *Genes Dev.*, **26**, 1703–1713.
21. Oganesian,L. and Karlseder,J. (2011) Mammalian 5' C-rich telomeric overhangs are a mark of recombination-dependent telomere maintenance. *Mol. Cell*, **42**, 224–236.
22. Baumann,P. and Cech,T.R. (2001) Pot1, the putative telomere end-binding protein in fission yeast and humans. *Science*, **292**, 1171–1175.
23. Cooper,J.P., Nimmo,E.R., Allshire,R.C. and Cech,T.R. (1997) Regulation of telomere length and function by a Myb-domain protein in fission yeast. *Nature*, **385**, 744–747.
24. Carneiro,T., Khair,L., Reis,C.C., Borges,V., Moser,B.A., Nakamura,T.M. and Ferreira,M.G. (2010) Telomeres avoid end detection by severing the checkpoint signal transduction pathway. *Nature*, **467**, 228–232.
25. Gao,H., Cervantes,R.B., Mandell,E.K., Otero,J.H. and Lundblad,V. (2007) RPA-like proteins mediate yeast telomere function. *Nat. Struct. Mol. Biol.*, **14**, 208–214.
26. Sun,J., Yu,E.Y., Yang,Y., Confer,L.A., Sun,S.H., Wan,K., Lue,N.F. and Lei,M. (2009) Stn1-Ten1 is an Rpa2-Rpa3-like complex at telomeres. *Genes Dev.*, **23**, 2900–2914.
27. Miyake,Y., Nakamura,M., Nabetani,A., Shimamura,S., Tamura,M., Yonehara,S., Saito,M. and Ishikawa,F. (2009) RPA-like mammalian Ctc1-Stn1-Ten1 complex binds to single-stranded DNA and protects telomeres independently of the Pot1 pathway. *Mol. Cell*, **36**, 193–206.
28. Surovtseva,Y.V., Churikov,D., Boltz,K.A., Song,X., Lamb,J.C., Warrington,R., Leehy,K., Heacock,M., Price,C.M. and Shippen,D.E. (2009) Conserved telomere maintenance component 1 interacts with STN1 and maintains chromosome ends in higher eukaryotes. *Mol. Cell*, **36**, 207–218.
29. Chen,L.Y., Redon,S. and Lingner,J. (2012) The human CST complex is a terminator of telomerase activity. *Nature*, **488**, 540–544.
30. Stewart,J.A., Wang,F., Chaiken,M.F., Kasbek,C., Chastain,P.D., Wright,W.E. and Price,C.M. (2012) Human CST promotes telomere duplex replication and general replication restart after fork stalling. *EMBO J.*, **31**, 3537–3549.
31. Kasbek,C., Wang,F. and Price,C.M. (2013) Human TEN1 maintains telomere integrity and functions in genome-wide replication restart. *J. Biol. Chem.*, **288**, 30139–30150.
32. Raffa,G.D., Ciapponi,L., Cenci,G. and Gatti,M. (2011) Terminin: a protein complex that mediates epigenetic maintenance of Drosophila telomeres. *Nucleus*, **2**, 383–391.
33. Mason,J.M., Randall,T.A. and Capkova Frydrychova,R. (2015) Telomerase lost?. *Chromosoma*, **125**, 65–73.
34. Pardue,M.L. and DeBaryshe,P.G. (2008) Drosophila telomeres: A variation on the telomerase theme. *Fly (Austin)*, **2**, 101–110.
35. Zhang,L. and Rong,Y.S. (2012) Retrotransposons at Drosophila telomeres: Host domestication of a selfish element for the maintenance of genome integrity. *Biochim. Biophysi. Acta*, **1819**, 771–775.
36. Biessmann,H., Carter,S.B. and Mason,J.M. (1990) Chromosome ends in Drosophila without telomeric DNA sequences. *Proc. Natl. Acad. Sci. U.S.A.*, **87**, 1758–1761.
37. Levis,R.W. (1989) Viable deletions of a telomere from a Drosophila chromosome. *Cell*, **58**, 791–801.
38. Rong,Y.S. (2008) Telomere capping in Drosophila: dealing with chromosome ends that most resemble DNA breaks. *Chromosoma*, **117**, 235–242.
39. Raffa,G.D., Siriaco,G., Cugusi,S., Ciapponi,L., Cenci,G., Wojcik,E. and Gatti,M. (2009) The Drosophila modigliani (moi) gene encodes a HOAP-interacting protein required for telomere protection. *Proc. Natl. Acad. Sci. U.S.A.*, **106**, 2271–2276.
40. Raffa,G.D., Raimondo,D., Sorino,C., Cugusi,S., Cenci,G., Cacchione,S., Gatti,M. and Ciapponi,L. (2010) Verrocchio, a Drosophila OB fold-containing protein, is a component of the terminin telomere-capping complex. *Genes Dev.*, **24**, 1596–1601.
41. Raffa,G.D., Cenci,G., Ciapponi,L. and Gatti,M. (2013) Organization and evolution of Drosophila terminin: similarities and differences between Drosophila and human telomeres. *Front. Oncol.*, **3**, 112.
42. Gao,G., Walser,J.C., Beaucher,M.L., Morciano,P., Wesolowska,N., Chen,J. and Rong,Y.S. (2010) HipHop interacts with HOAP and HP1 to protect Drosophila telomeres in a sequence-independent manner. *EMBO J.*, **29**, 819–829.
43. Zhang,L., Beaucher,M., Cheng,Y. and Rong,Y.S. (2014) Coordination of transposon expression with DNA replication in the targeting of telomeric retrotransposons in Drosophila. *EMBO J.*, **33**, 1148–1158.
44. Pisano,S., Marchioni,E., Galati,A., Mechelli,R., Savino,M. and Cacchione,S. (2007) Telomeric nucleosomes are intrinsically mobile. *J. Mol. Biol.*, **369**, 1153–1162.
45. Poulet,A., Pisano,S., Faivre-Moskalenko,C., Pei,B., Tauran,Y., Haftek-Terreau,Z., Brunet,F., Le Bihan,Y.V., Ledu,M.H., Montel,F. *et al.* (2012) The N-terminal domains of TRF1 and TRF2 regulate their ability to condense telomeric DNA. *Nucleic Acids Res.*, **40**, 2566–2576.
46. Bustamante,C. and Rivetti,C. (1996) Visualizing protein-nucleic acid interactions on a large scale with the scanning force microscope. *Annu. Rev. Biophys. Biomol. Struct.*, **25**, 395–429.
47. Pisano,S., Leoni,D., Galati,A., Rhodes,D., Savino,M. and Cacchione,S. (2010) The human telomeric protein hTRF1 induces telomere-specific nucleosome mobility. *Nucleic Acids Res.*, **38**, 2247–2255.
48. Amiard,S., Doudeau,M., Pinte,S., Poulet,A., Lenain,C., Faivre-Moskalenko,C., Angelov,D., Hug,N., Vindigni,A., Bouvet,P. *et al.* (2007) A topological mechanism for TRF2-enhanced strand invasion. *Nat. Struct. Mol. Biol.*, **14**, 147–154.
49. Shlyakhtenko,L.S., Lushnikov,A.Y., Miyagi,A. and Lyubchenko,Y.L. (2012) Specificity of binding of single-stranded DNA-binding protein to its target. *Biochemistry*, **51**, 1500–1509.
50. Cenci,G., Siriaco,G., Raffa,G.D., Kellum,R. and Gatti,M. (2003) The Drosophila HOAP protein is required for telomere capping. *Nat. Cell Biol.*, **5**, 82–84.
51. Raffa,G.D., Cenci,G., Siriaco,G., Goldberg,M.L. and Gatti,M. (2005) The putative Drosophila transcription factor woc is required to prevent telomeric fusions. *Mol. Cell*, **20**, 821–831.
52. Palumbo,V., Pellacani,C., Heesom,K.J., Rogala,K.B., Deane,C.M., Mottier-Pavie,V., Gatti,M., Bonaccorsi,S. and Wakefield,J.G. (2015) Misato controls mitotic microtubule generation by stabilizing the TCP-1 tubulin chaperone complex. *Curr. Biol.: CB*, **25**, 1777–1783.
53. Deckmann,K., Rorsch,F., Geisslinger,G. and Grosch,S. (2012) Identification of DNA-protein complexes using an improved, combined western blotting-electrophoretic mobility shift assay (WEMSA) with a fluorescence imaging system. *Mol. Biosyst.*, **8**, 1389–1395.
54. Moeenrezakhanlou,A., Nandan,D. and Reiner,N.E. (2008) Identification of a calcitriol-regulated Sp-1 site in the promoter of human CD14 using a combined western blotting electrophoresis mobility shift assay (WEMSA). *Biol. Proc. Online*, **10**, 29–35.
55. Pisano,S., Pascucci,E., Cacchione,S., De Santis,P. and Savino,M. (2006) AFM imaging and theoretical modeling studies of sequence-dependent nucleosome positioning. *Biophys. Chem.*, **124**, 81–89.
56. Lohman,T.M. and Ferrari,M.E. (1994) Escherichia coli single-stranded DNA-binding protein: multiple DNA-binding modes and cooperativities. *Annu. Rev. Biochem.*, **63**, 527–570.
57. Schneider,S.W., Larmer,J., Henderson,R.M. and Oberleithner,H. (1998) Molecular weights of individual proteins correlate with

molecular volumes measured by atomic force microscopy. *Pflugers Arch.*, **435**, 362–367.
58. de Vries,S.J. and Bonvin,A.M. (2011) CPORT: a consensus interface predictor and its performance in prediction-driven docking with HADDOCK. *PLoS One*, **6**, e17695.
59. Zhang,Y., Zhang,L., Tang,X., Bhardwaj,S.R., Ji,J. and Rong,Y.S. (2016) MTV, an ssDNA protecting complex essential for transposon-based telomere maintenance in Drosophila. *PLoS Genet.*, **12**, e1006435.
60. Flynn,R.L., Centore,R.C., O'Sullivan,R.J., Rai,R., Tse,A., Songyang,Z., Chang,S., Karlseder,J. and Zou,L. (2011) TERRA and hnRNPA1 orchestrate an RPA-to-POT1 switch on telomeric single-stranded DNA. *Nature*, **471**, 532–536.
61. Lake,C.M., Holsclaw,J.K., Bellendir,S.P., Sekelsky,J. and Hawley,R.S. (2013) The development of a monoclonal antibody recognizing the Drosophila melanogaster phosphorylated histone H2A variant (gamma-H2AV). *G3*, **3**, 1539–1543.
62. Andreyeva,E.N., Kolesnikova,T.D., Belyaeva,E.S., Glaser,R.L. and Zhimulev,I.F. (2008) Local DNA underreplication correlates with accumulation of phosphorylated H2Av in the Drosophila melanogaster polytene chromosomes. *Chromosome Res*, **16**, 851–862.
63. Thanasoula,M., Escandell,J.M., Martinez,P., Badie,S., Munoz,P., Blasco,M.A. and Tarsounas,M. (2010) p53 prevents entry into mitosis with uncapped telomeres. *Curr. Biol.: CB*, **20**, 521–526.
64. Hayashi,M.T., Cesare,A.J., Fitzpatrick,J.A., Lazzerini-Denchi,E. and Karlseder,J. (2012) A telomere-dependent DNA damage checkpoint induced by prolonged mitotic arrest. *Nat. Struct. Mol. Biol.*, **19**, 387–394.
65. Kim,J.A., Kruhlak,M., Dotiwala,F., Nussenzweig,A. and Haber,J.E. (2007) Heterochromatin is refractory to gamma-H2AX modification in yeast and mammals. *J. Cell Biol.*, **178**, 209–218.
66. Zou,L. and Elledge,S.J. (2003) Sensing DNA damage through ATRIP recognition of RPA-ssDNA complexes. *Science*, **300**, 1542–1548.
67. Flynn,R.L., Chang,S. and Zou,L. (2012) RPA and POT1: friends or foes at telomeres? *Cell Cycle*, **11**, 652–657.
68. Luciano,P., Coulon,S., Faure,V., Corda,Y., Bos,J., Brill,S.J., Gilson,E., Simon,M.N. and Geli,V. (2012) RPA facilitates telomerase activity at chromosome ends in budding and fission yeasts. *EMBO J.*, **31**, 2034–2046.
69. Capkova Frydrychova,R., Biessmann,H. and Mason,J.M. (2008) Regulation of telomere length in Drosophila. *Cytogenetic Genome Res.*, **122**, 356–364.
70. Dickey,T.H., McKercher,M.A. and Wuttke,D.S. (2013) Nonspecific recognition is achieved in Pot1pC through the use of multiple binding modes. *Structure*, **21**, 121–132.
71. Mandell,E.K., Gelinas,A.D., Wuttke,D.S. and Lundblad,V. (2011) Sequence-specific binding to telomeric DNA is not a conserved property of the Cdc13 DNA binding domain. *Biochemistry*, **50**, 6289–6291.
72. Shareef,M.M., King,C., Damaj,M., Badagu,R., Huang,D.W. and Kellum,R. (2001) Drosophila heterochromatin protein 1 (HP1)/origin recognition complex (ORC) protein is associated with HP1 and ORC and functions in heterochromatin-induced silencing. *Mol. Biol. Cell*, **12**, 1671–1685.
73. Kim,C., Snyder,R.O. and Wold,M.S. (1992) Binding properties of replication protein A from human and yeast cells. *Mol. Cell. Biol.*, **12**, 3050–3059.
74. Pinzaru,A.M., Hom,R.A., Beal,A., Phillips,A.F., Ni,E., Cardozo,T., Nair,N., Choi,J., Wuttke,D.S., Sfeir,A. *et al.* (2016) Telomere replication stress induced by POT1 inactivation accelerates tumorigenesis. *Cell Rep.*, **15**, 2170–2184.
75. Lei,M., Podell,E.R. and Cech,T.R. (2004) Structure of human POT1 bound to telomeric single-stranded DNA provides a model for chromosome end-protection. *Nat. Struct. Mol. Biol.*, **11**, 1223–1229.
76. Lue,N.F. (2010) Plasticity of telomere maintenance mechanisms in yeast. *Trends Biochem. Sci.*, **35**, 8–17.
77. Lewis,K.A. and Wuttke,D.S. (2012) Telomerase and telomere-associated proteins: structural insights into mechanism and evolution. *Structure*, **20**, 28–39.
78. Giraud-Panis,M.J., Pisano,S., Benarroch-Popivker,D., Pei,B., Le Du,M.H. and Gilson,E. (2013) One identity or more for telomeres? *Front. Oncol.*, **3**, 48.
79. Lloyd,N.R., Dickey,T.H., Hom,R.A. and Wuttke,D.S. (2016) Tying up the ends: plasticity in the recognition of ssDNA at telomeres. *Biochemistry*, **55**, 5326–5340.
80. Linger,B.R. and Price,C.M. (2009) Conservation of telomere protein complexes: shuffling through evolution. *Crit. Rev. Biochem. Mol. Biol.*, **44**, 434–446.
81. Cipressa,F., Morciano,P., Bosso,G., Mannini,L., Galati,A., Daniela Raffa,G., Cacchione,S., Musio,A. and Cenci,G. (2016) A role for Separase in telomere protection. *Nat. Commun.*, **7**, 10405.
82. Cenci,G., Ciapponi,L., Marzullo,M., Raffa,G.D., Morciano,P., Raimondo,D., Burla,R., Saggio,I. and Gatti,M. (2015) The analysis of pendolino (peo) mutants reveals differences in the fusigenic potential among Drosophila telomeres. *PLoS Genet.*, **11**, e1005260.
83. Burla,R., Carcuro,M., Raffa,G.D., Galati,A., Raimondo,D., Rizzo,A., La Torre,M., Micheli,E., Ciapponi,L., Cenci,G. *et al.* (2015) AKTIP/Ft1, a new shelterin-interacting factor required for telomere maintenance. *PLoS Genet.*, **11**, e1005167.